E. M. Dean

ANL-7673

Argonne National Laboratory

THE INFLUENCE OF A PREDOMINANTLY OXIDE FUEL LOADING ON THE DYNAMIC BEHAVIOR OF EBR-II

by

A. V. Campise

The facilities of Argonne National Laboratory are owned by the United States Government. Under the terms of a contract (W-31-109-Eng-38) between the U. S. Atomic Energy Commission, Argonne Universities Association and The University of Chicago, the University employs the staff and operates the Laboratory in accordance with policies and programs formulated, approved and reviewed by the Association.

MEMBERS OF ARGONNE UNIVERSITIES ASSOCIATION

The University of Arizona
Carnegie-Mellon University
Case Western Reserve University
The University of Chicago
University of Cincinnati
Illinois Institute of Technology
University of Illinois
Indiana University
Iowa State University
The University of Iowa
Kansas State University
The University of Kansas
Loyola University
Marquette University
Michigan State University
The University of Michigan
University of Minnesota
University of Missouri
Northwestern University
University of Notre Dame
The Ohio State University
Ohio University
The Pennsylvania State University
Purdue University
Saint Louis University
Southern Illinois University
The University of Texas at Austin
Washington University
Wayne State University
The University of Wisconsin

NOTICE

This report was prepared as an account of work sponsored by the United States Government. Neither the United States nor the United States Atomic Energy Commission, nor any of their employees, nor any of their contractors, subcontractors, or their employees, makes any warranty, express or implied, or assumes any legal liability or responsibility for the accuracy, completeness or usefulness of any information, apparatus, product or process disclosed, or represents that its use would not infringe privately-owned rights.

Printed in the United States of America
Available from
National Technical Information Service
U.S. Department of Commerce
5285 Port Royal Road
Springfield, Virginia 22151
Price: Printed Copy $3.00; Microfiche $0.95

ANL-7673
Reactor Technology

ARGONNE NATIONAL LABORATORY
9700 South Cass Avenue
Argonne, Illinois 60439

THE INFLUENCE OF A PREDOMINANTLY OXIDE FUEL LOADING ON THE DYNAMIC BEHAVIOR OF EBR-II

by

A. V. Campise

EBR-II Project

October 1970

TABLE OF CONTENTS

	Page
ABSTRACT	15
I. INTRODUCTION	15
II. TRENDS IN EBR-II IRRADIATION-CORE LOADINGS	17
III. DYNAMIC SIMULATION OF REACTOR-CORE LOADINGS	23
A. Assumptions	23
B. Dynamic Models	23
1. Rod-drop Experiments	23
2. Dynamic System Analysis	26
C. Limitations	29
IV. FUNDAMENTAL DYNAMIC BEHAVIOR OF OXIDE AND METALLIC FUEL ELEMENTS	30
A. Physical Properties of Fuel Elements	30
B. General Dynamic Behavior	33
C. The Effect of Thermal Conductivity on Dynamic Response	35
D. The Effect of Specific Heat on Dynamic Response	44
E. Summary	48
V. DYNAMIC BEHAVIOR DURING NORMAL REACTOR OPERATIONS	49
A. Rod-drop Experiments	49
B. Reactor Trips	54
VI. DYNAMIC BEHAVIOR DURING OPERATIONAL ABNORMALITIES	57
A. Full-power Operations	57
B. Startup	60

TABLE OF CONTENTS

Page

VII. SUMMARY AND CONCLUSIONS 79

APPENDIXES

A. Fuel-handling Malfunctions 80

1. Insertion of Central Subassembly at High Speed. 80
2. Insertion of Central Subassembly at Low Speed 80
3. Dropping of a Central Subassembly 84

B. Reactor-kinetics Data 88

ACKNOWLEDGMENT 89

REFERENCES 90

LIST OF FIGURES

No.	Title	Page
1.	Number of In-core Experimental Subassemblies as a Function of Years of EBR-II Operation as the AEC LMFBR Irradiation Facility	17
2.	Core-loading Pattern for Run 4	18
3.	Core-loading Pattern for Run 7	19
4.	Core-loading Pattern for Run 14	20
5.	Core-loading Pattern for Run 29A	21
6.	Core-loading Pattern for Run 38B	22
7.	Feedback Network for Simulating the Closed-loop Behavior of EBR-II during Rod-drop Experiments	24
8.	Eight-channel Representation of EBR-II Core and Blanket for Feedback Modeling for Rod-drop Experiments	25
9.	Feedback Network for Simulating the Closed-loop Behavior of EBR-II with a Predominantly Oxide Loading	27
10.	Seven-channel Representation of EBR-II Core and Blanket for Feedback Modeling of a Predominantly Oxide Loading	28
11.	Thermal Conductivity of Uranium-5 wt % Fissium and PuO_2-UO_2 as a Function of Temperature	31
12.	Specific Heat of Uranium-5 wt % Fissium and PuO_2-UO_2 as a Function of Temperature	32
13.	Transient Response of Oxide Fuel Elements following an Accidental Insertion of Reactivity at a Ramp Rate of 5$/sec into a Just-critical Core, Showing Variations due to Assumed Thermal Conductivities of Oxide Fuel	33
14.	Transient Response of Oxide Fuel Elements following an Accidental Insertion of Reactivity at a Ramp Rate of 5$/sec into a Just-critical Core, Showing Variations due to Assumed Specific Heats of Oxide Fuel	34
15.	Peak Fuel Temperatures following an Inadvertent Insertion of Reactivity at a Ramp Rate of 10$/sec into a Just-critical Core under Conditions of Full Primary-coolant Flow, Using Measured k and C_p for Oxide Fuel	36
16.	Peak Fuel Temperatures following an Inadvertent Insertion of Reactivity at a Ramp Rate of 1.0$/sec into a Just-critical Core under Conditions of Full Primary-coolant Flow, Using Measured k and C_p for Oxide Fuel	37

LIST OF FIGURES

No.	Title	Page
17.	Peak Fuel Temperatures following an Inadvertent Insertion of Reactivity at a Ramp Rate of 0.1$/sec into a Just-critical Core under Conditions of Full Primary-coolant Flow, Using Measured k and C_p for Oxide Fuel	38
18.	Peak Fuel Temperatures following an Inadvertent Insertion of Reactivity at a Ramp Rate of 0.01$/sec into a Just-critical Core under Conditions of Full Primary-coolant Flow, Using Measured k and C_p for Oxide Fuel	39
19.	Peak Fuel Temperatures for Various Reactivity Ramp Rates, Using Measured k and C_p for Oxide Fuel	40
20.	Peak Fuel Temperatures following an Inadvertent Insertion of Reactivity at a Ramp Rate of 10$/sec into a Just-critical Core under Conditions of Full Primary-coolant Flow, Using Measured C_p and Oxide k = Metal k	40
21.	Peak Fuel Temperatures following an Inadvertent Insertion of Reactivity at a Ramp Rate of 1.0$/sec into a Just-critical Core under Conditions of Full Primary-coolant Flow, Using Measured C_p and Oxide k = Metal k	41
22.	Peak Fuel Temperatures Following an Inadvertent Insertion of Reactivity at a Ramp Rate of 0.1$/sec into a Just-critical Core under Conditions of Full Primary-coolant Flow, Using Measured C_p and Oxide k = Metal k	42
23.	Peak Fuel Temperatures following an Inadvertent Insertion of Reactivity at a Ramp Rate of 0.01$/sec into a Just-critical Core under Conditions of Full Primary-coolant Flow, Using Measured C_p and Oxide k = Metal k	43
24.	Peak Fuel Temperatures for Various Reactivity Ramp Rates, Using Measured C_p and Oxide k = Metal k	44
25.	Peak Fuel Temperatures following an Inadvertent Insertion of Reactivity at a Ramp Rate of 10$/sec into a Just-critical Core under Conditions of Full Primary-coolant Flow, Using Measured k and Oxide C_p = Metal C_p	45
26.	Peak Fuel Temperatures following an Inadvertent Insertion of Reactivity at a Ramp Rate of 1.0$/sec into a Just-critical Core under Conditions of Full Primary-coolant Flow, Using Measured k and Oxide C_p = Metal C_p	46

LIST OF FIGURES

No.	Title	Page
27.	Peak Fuel Temperatures following an Inadvertent Insertion of Reactivity at a Ramp Rate of 0.1$/sec into a Just-critical Core under Conditions of Full Primary-coolant Flow, Using Measured k and Oxide C_p = Metal C_p	46
28.	Peak Fuel Temperatures Following an Inadvertent Insertion of Reactivity at a Ramp Rate of 0.01$/sec into a Just-critical Core under Conditions of Full Primary-coolant Flow, Using Measured k and Oxide C_p = Metal C_p	47
29.	Peak Fuel Temperatures for Various Reactivity Ramp Rates, Using Measured k and Oxide C_p = Metal C_p	48
30.	Power and Reactivity Feedback following a Rod-drop Experiment at 50 MWt in a Typical Present Core Loading, with Only Driver-fuel and Sodium-coolant Feedback	50
31.	Power and Reactivity Feedback following a Rod-drop Experiment at 50 MWt in a Predominantly Oxide-fuel Core, with Only Sodium-coolant Feedback	50
32.	Power and Reactivity Feedback following a Rod-drop Experiment at 50 MWt in a Predominantly Oxide-fuel Core, Assuming Feedback from Oxide-fuel Axial Expansion and Sodium-density Changes	52
33.	Power and Reactivity Feedback following a Rod-drop Experiment at 50 MWt in a Predominantly Oxide-fuel Core, Assuming Feedback from Reduced Oxide-fuel Axial Expansion and Normal Sodium-density Changes	52
34.	Power and Reactivity Feedback following a Rod-drop Experiment at 50 MWt in a Predominantly Oxide-fuel Core, Assuming Oxide-fuel Doppler Constant = -0.001 and Sodium-density Changes	53
35.	Power and Reactivity Feedback following a Rod-drop Experiment at 50 MWt in a Predominantly Oxide-fuel Core, Assuming Feedback from Sodium-density Changes and Oxide-fuel Axial Expansion = Metal-fuel Axial Expansion	53
36.	Fuel Temperatures following the Insertion of Reactivity at a Ramp Rate of 1.0$/sec, Followed by a Reactor Trip at 1.5 sec after Start of Insertion	55
37.	Sodium-coolant Outlet Temperatures following the Insertion of Reactivity at a Ramp Rate of 1.0$/sec, Followed by a Reactor Trip at 1.5 sec after Start of Insertion	56

LIST OF FIGURES

No.	Title	Page
38.	Time to Centerline Melting in Average Oxide Element, Assuming Various Metal-core Feedbacks	57
39.	Time to Centerline Melting in Average Oxide Element, Assuming Various Oxide-core Feedbacks	58
40.	Time to Centerline Melting in Average Oxide Element, Assuming Various Feedbacks from Oxide Doppler and from Metal Fuel (sodium feedback included in all cases)	59
41.	Power and Reactivity Curves following the Driving of a Control Rod into a Just-critical Core; Doppler Constant = -0.0005; Half of Metal-fuel Feedback; Full Coolant Flow	61
42.	Temperatures in Peak Driver-fuel Element following the Driving of a Control Rod into a Just-critical Core; Doppler Constant = -0.0005; Half of Metal-fuel Feedback; Full Coolant Flow	61
43.	Temperatures in Peak Oxide-fuel Element following the Driving of a Control Rod into a Just-critical Core; Doppler Constant = -0.0005; Half of Metal-fuel Feedback; Full Coolant Flow	62
44.	Temperatures in Average Oxide-fuel Element following the Driving of a Control Rod into a Just-critical Core; Doppler Constant = -0.0005; Half of Metal-fuel Feedback; Full Coolant Flow	63
45.	Power and Reactivity Curves following the Driving of a Control Rod into a Just-critical Core; Doppler Constant = -0.001; No Metal-fuel Feedback; Full Coolant Flow	63
46.	Temperatures in Peak Driver-fuel Element following the Driving of a Control Rod into a Just-critical Core; Doppler Constant = -0.001; No Metal-fuel Feedback; Full Coolant Flow	64
47.	Temperatures in Peak Oxide-fuel Element following the Driving of a Control Rod into a Just-critical Core; Doppler Constant = -0.001; No Metal-fuel Feedback; Full Coolant Flow	64
48.	Temperatures in Average Oxide-fuel Element following the Driving of a Control Rod into a Just-critical Core; Doppler Constant = -0.001; No Metal-fuel Feedback; Full Coolant Flow	65

LIST OF FIGURES

No.	Title	Page
49.	Power and Reactivity Curves following the Driving of a Control Rod into a Just-critical Core; Doppler Constant = -0.002; Half of Metal-fuel Feedback; Full Coolant Flow	65
50.	Temperatures in Peak Driver-fuel Element following the Driving of a Control Rod into a Just-critical Core; Doppler Constant = -0.002; Half of Metal-fuel Feedback; Full Coolant Flow	66
51.	Temperatures in Peak Oxide-fuel Element following the Driving of a Control Rod into a Just-critical Core; Doppler Constant = -0.002; Half of Metal-fuel Feedback; Full Coolant Flow	67
52.	Temperatures in Average Oxide-fuel Element following the Driving of a Control Rod into a Just-critical Core; Doppler Constant = -0.002; Half of Metal-fuel Feedback; Full Coolant Flow	67
53.	Power and Reactivity Curves following the Driving of a Control Rod into a Just-critical Core; Doppler Constant = -0.004; No Metal-fuel Feedback; Full Coolant Flow	68
54.	Temperatures in Peak Driver-fuel Element following the Driving of a Control Rod into a Just-critical Core; Doppler Constant = -0.004; No Metal-fuel Feedback; Full Coolant Flow	68
55.	Temperatures in Peak Oxide-fuel Element following the Driving of a Control Rod into a Just-critical Core; Doppler Constant = -0.004; No Metal-fuel Feedback; Full Coolant Flow	69
56.	Temperatures in Average Oxide-fuel Element following the Driving of a Control Rod into a Just-critical Core; Doppler Constant = -0.004; No Metal-fuel Feedback; Full Coolant Flow	69
57.	Power and Reactivity Curves following the Driving of the Safety Rods into a Just-critical Core; Doppler Constant = -0.0005; Half of Metal-fuel Feedback; Full Coolant Flow	70
58.	Temperatures in Peak Driver-fuel Element following the Driving of the Safety Rods into a Just-critical Core; Doppler Constant = -0.0005; Half of Metal-fuel Feedback; Full Coolant Flow	70

LIST OF FIGURES

No.	Title	Page
59.	Temperatures in Peak Oxide-fuel Element following the Driving of the Safety Rods into a Just-critical Core; Doppler Constant = -0.0005; Half of Metal-fuel Feedback; Full Coolant Flow	71
60.	Temperatures in Average Oxide-fuel Element following the Driving of the Safety Rods into a Just-critical Core; Doppler Constant = -0.0005; Half of Metal-fuel Feedback; Full Coolant Flow	71
61.	Power and Reactivity Curves following the Driving of the Safety Rods into a Just-critical Core; Doppler Constant = -0.001; No Metal-fuel Feedback; Full Coolant Flow	72
62.	Temperatures in Peak Driver-fuel Element following the Driving of the Safety Rods into a Just-critical Core; Doppler Constant = -0.001; No Metal-fuel Feedback; Full Coolant Flow	73
63.	Temperatures in Peak Oxide-fuel Element following the Driving of the Safety Rods into a Just-critical Core; Doppler Constant = -0.001; No Metal-fuel Feedback; Full Coolant Flow	74
64.	Temperatures in Average Oxide-fuel Element following the Driving of the Safety Rods into a Just-critical Core; Doppler Constant = -0.001; No Metal-fuel Feedback; Full Coolant Flow	74
65.	Power and Reactivity Curves following the Driving of the Safety Rods into a Just-critical Core; Doppler Constant = -0.002; Half of Metal-fuel Feedback; Full Coolant Flow	75
66.	Temperatures in Peak Driver-fuel Element following the Driving of the Safety Rods into a Just-critical Core; Doppler Constant = -0.002; Half of Metal-fuel Feedback; Full Coolant Flow	75
67.	Temperatures in Peak Oxide-fuel Element following the Driving of the Safety Rods into a Just-critical Core; Doppler Constant = -0.002; Half of Metal-fuel Feedback; Full Coolant Flow	76
68.	Temperatures in Average Oxide-fuel Element following the Driving of the Safety Rods into a Just-critical Core; Doppler Constant = -0.002; Half of Metal-fuel Feedback; Full Coolant Flow	76

LIST OF FIGURES

No.	Title	Page
69.	Power and Reactivity Curves following the Driving of the Safety Rods into a Just-critical Core; Doppler Constant = -0.004; No Metal-fuel Feedback; Full Coolant Flow	77
70.	Temperatures in Peak Driver-fuel Element following the Driving of the Safety Rods into a Just-critical Core; Doppler Constant = -0.004; No Metal-fuel Feedback; Full Coolant Flow	77
71.	Temperatures in Peak Oxide-fuel Element following the Driving of the Safety Rods into a Just-critical Core; Doppler Constant = -0.004; No Metal-fuel Feedback; Full Coolant Flow	78
72.	Temperatures in Average Oxide-fuel Element following the Driving of the Safety Rods into a Just-critical Core; Doppler Constant = -0.004; No Metal-fuel Feedback; Full Coolant Flow	78
73.	Power and Reactivity Curves following the Driving of a Central Subassembly at High Speed into a Just-critical Core; Doppler Constant = -0.0005; Half of Metal-fuel Feedback; Reduced Coolant Flow	81
74.	Temperatures in Peak Driver-fuel Element following the Driving of a Central Subassembly at High Speed into a Just-critical Core; Doppler Constant = -0.0005; Half of Metal-fuel Feedback; Reduced Coolant Flow	81
75.	Temperatures in Peak Oxide-fuel Subassembly following the Driving of a Central Subassembly at High Speed into a Just-critical Core; Doppler Constant = -0.0005; Half of Metal-fuel Feedback; Reduced Coolant Flow	82
76.	Temperatures in Average Oxide-fuel Subassembly following the Driving of a Central Subassembly at High Speed into a Just-critical Core; Doppler Constant = -0.0005; Half of Metal-fuel Feedback; Reduced Coolant Flow	82
77.	Power and Reactivity Curves following the Driving of a Central Subassembly at Low Speed into a Just-critical Core; Doppler Constant = -0.002; Half of Metal-fuel Feedback; Reduced Coolant Flow	83
78.	Temperatures in Peak Driver-fuel Element following the Driving of a Central Subassembly at Low Speed into a Just-critical Core; Doppler Constant = -0.002; Half of Metal-fuel Feedback; Reduced Coolant Flow	83

LIST OF FIGURES

No.	Title	Page
79.	Temperatures in Peak Oxide-fuel Element following the Driving of a Central Subassembly at Low Speed into a Just-critical Core; Doppler Constant = -0.002; Half of Metal-fuel Feedback; Reduced Coolant Flow	84
80.	Temperatures in Average Oxide-fuel Subassembly following the Driving of a Central Subassembly at Low Speed into a Just-critical Core; Doppler Constant = -0.002; Half of Metal-fuel Feedback; Reduced Coolant Flow	84
81.	Power and Reactivity Curves following the Dropping of a Central Subassembly into a Just-critical Core; Doppler Constant = -0.002; Half of Metal-fuel Feedback; Reduced Coolant Flow	85
82.	Temperatures in Peak Driver-fuel Element following the Dropping of a Central Subassembly into a Just-critical Core; Doppler Constant = -0.002; Half of Metal-fuel Feedback; Reduced Coolant Flow	86
83.	Temperatures in Peak Oxide-fuel Element following the Dropping of a Central Subassembly into a Just-critical Core; Doppler Constant = -0.002; Half of Metal-fuel Feedback; Reduced Coolant Flow	86
84.	Temperatures in Average Oxide-fuel Element following the Dropping of a Central Subassembly into a Just-critical Core; Doppler Constant = -0.002; Half of Metal-fuel Feedback; Reduced Coolant Flow	87

LIST OF TABLES

No.	Title	Page
I.	Data for EBR-II Run 4 (72-subassembly core size)	18
II.	Data for EBR-II Run 7 (74-subassembly core size)	19
III.	Data for EBR-II Run 14 (80-subassembly core size)	20
IV.	Data for EBR-II Run 29A (87-subassembly core size)	21
V.	Data for EBR-II Run 38B (90-subassembly core size)	22
VI.	Seven-channel Model Used in the Dynamic System Analysis of Predominantly Oxide Fuel Loadings in EBR-II	30
VII.	Assumed Physical Properties of Typical Fuel Elements	32
VIII.	Nine-channel Model Used in Dynamic Simulation of EBR-II Rod-drop Experiments	49
IX.	Comparison of Rod-drop Experiments Assuming Several Different Types of Reactivity-feedback Sources	54
X.	Range of Temperature-induced Feedback Parameters Used in Dynamic Analysis	60
XI.	Comparison of Various Reactivity-feedback Effects on Peak Fuel-element Temperatures following an Inadvertent Driving In of a Control Rod during Reactor Startup	72
XII.	Comparison of Various Reactivity-feedback Effects on Peak Fuel-element Temperatures following an Inadvertent Driving In of the Safety Rods during Reactor Startup	73
XIII.	Comparison of Various Reactivity-feedback Effects on Peak Fuel-element Temperatures following Fuel-handling Malfunctions	87
XIV.	Effective Delayed-neutron Constants	88

THE INFLUENCE OF A PREDOMINANTLY OXIDE FUEL LOADING ON THE DYNAMIC BEHAVIOR OF EBR-II

by

A. V. Campise

ABSTRACT

The AIROS-IIA dynamic-simulation digital code was used to study the behavior of future EBR-II cores containing predominantly oxide fuel. This study completes a survey of the response of EBR-II to hypothetical malfunctions of components. Previous studies, as well as operating experience at EBR-II, have been with loadings of predominantly metallic driver fuel. The response of this fuel to a variety of operating conditions has been well documented. Future loadings, however, are expected to contain an increasingly higher proportion of experimental oxide fuels. The present study considers the response of predominantly oxide cores with and without Doppler feedbacks. The study concludes that the future dynamic behavior of EBR-II with loadings of predominantly oxide fuel is predictable, safe, and well within the range of present operating experience.

I. INTRODUCTION

EBR-II,* currently the principal LMFBR irradiation facility, was originally designed as an engineering facility to demonstrate the engineering and operating feasibility of sodium-cooled fast breeder reactors as applied to the design of central-station power plants.[1,2] In the natural evolution of the LMFBR program, the need for a fast-neutron irradiation facility was identified, and the primary objective of EBR-II was changed to meet this need.

Many years of operating experience have been gained with EBR-II core loadings composed predominantly of metallic driver-fuel elements containing uranium-5 wt % fissium. The dynamic behavior of the EBR-II core with a predominantly metallic fuel loading is well understood and documented. The change in the EBR-II objective to that of a fast-neutron

*Experimental Breeder Reactor II (EBR-II) is the United States Atomic Energy Commission's primary facility for irradiation tests of fuels and materials in the Liquid Metal Fast Breeder Reactor (LMFBR) Program.

irradiation facility has called for a gradual reconfiguration in core loading, however. An increasing number of irradiation experiments containing ceramic fuel, mostly oxide, have been loaded into the reactor. The effect of these ceramic fuel elements has become important in relating the dynamic characteristics of future cores to earlier experience with metallic driver fuel.

This report presents the fundamental dynamic behavior of typical oxide and metallic fuel elements. The report also analyzes the dynamic characteristics of EBR-II cores with heavy loadings of oxide fuel elements and presents the differences to be expected, both during normal operations and during operational abnormalities in the reactor plant. The report covers the dynamic behavior of EBR-II during rod-drop experiments, during normal reactor trips, and during hypothetical malfunctions involving control and safety rods.

Various EBR-II core configurations are studied herein by assuming various feedback networks in the reactor system. The most important of these feedback networks involve linear axial fuel expansion and involve Doppler coefficient in oxide fuel. The overall characteristics of future cores loaded predominantly with oxide fuel are summarized with respect to variations expected from the present dynamic behavior of EBR-II.

II. TRENDS IN EBR-II IRRADIATION-CORE LOADINGS

The initial experimental subassemblies were loaded into EBR-II for fast-neutron irradiation in May 1965.[3] The irradiation-core loadings have subsequently varied according to experimental demands, plant maintenance, and the performance of special physics measurements. Figure 1 shows the number of in-core experimental subassemblies as a function of years of EBR-II operation as the principal LMFBR irradiation facility. Temporary variations in experimental core loadings were primarily due to physics measurements in response to reactor stability questions that arose during the operation of EBR-II with a stainless steel reflector. The second major type of variation included in Fig. 1 had to do with the identification of leaking fuel elements that were releasing activity into the reactor tank. The suspected subassemblies were unloaded in sequential batches to identify the source of the activity. Figures 2-6 and Tables I-V present typical trends in EBR-II irradiation core loadings.

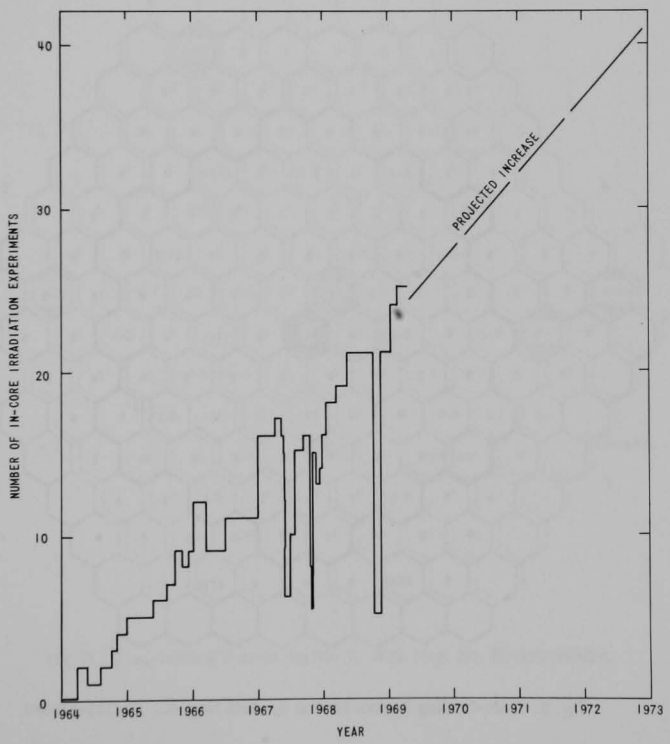

Fig. 1. Number of In-core Experimental Subassemblies as a Function of Years of EBR-II Operation as the AEC LMFBR Irradiation Facility. ANL Neg No. ID-103-M5682.

TABLE I. Data for EBR-II Run 4 (72-subassembly core size)

Chronology	
Date started	4/24/65
Date ended	5/4/65
Number of days for run	10
Power Data	
(A) Cumulative MWd(t) at start of run	1280
(B) Cumulative MWd(t) at end of run	1631
MWd(t) generated during run (B-A)	351
Types of Subassemblies in Core	
Blanket	11
Core	47
Control rod	12
Safety rod	2
Experimental (rows 1-6)	0
Experimental Subassemblies in Row 7	0

Key to Types of Subassemblies Shown in Loading Diagram (Fig. 2)

B--Depleted Uranium

BETH--Beryllium Thimble

C--Control Rod

D--Driver Fuel

S--Safety Rod

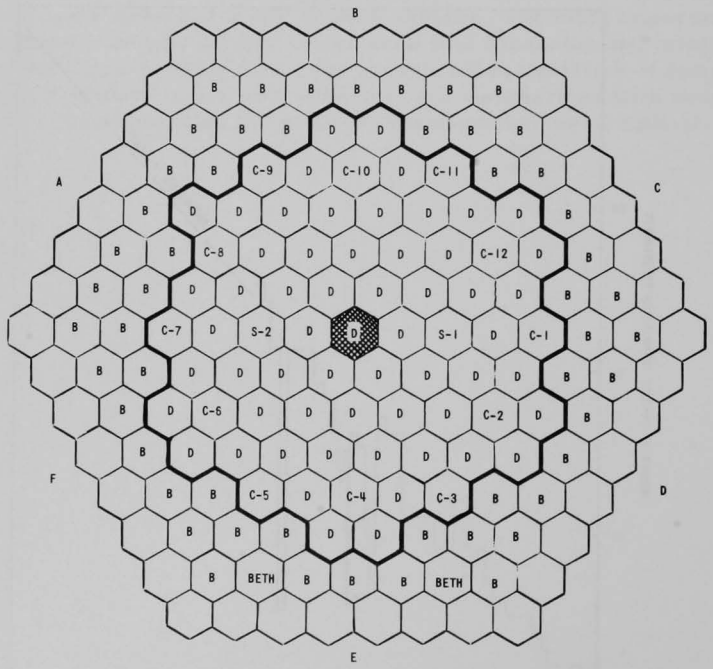

Fig. 2. Core-loading Pattern for Run 4. ANL Neg. No. ID-103-M5683.

TABLE II. Data for EBR-II Run 7 (74-subassembly core size)

Chronology	
Date started	7/29/65
Date ended	8/15/65
Number of days for run	17
Power Data	
(A) Cumulative MWd(t) at start of run	2502
(B) Cumulative MWd(t) at end of run	2927
MWd(t) generated during run (B-A)	425
Types of Subassemblies in Core	
Blanket	12
Core	47
Control rod	11
Safety rod	2
Experimental (rows 1-6)	1
Experimental Subassemblies in Row 7	3

Key to Types of Subassemblies Shown in Loading Diagram (Fig. 3)

B--Depleted Uranium

BETH--Beryllium Thimble

C--Control Rod

D--Driver Fuel

S--Safety Rod

SSCR--Stainless Steel Control Rod

X--Experimental Subassembly

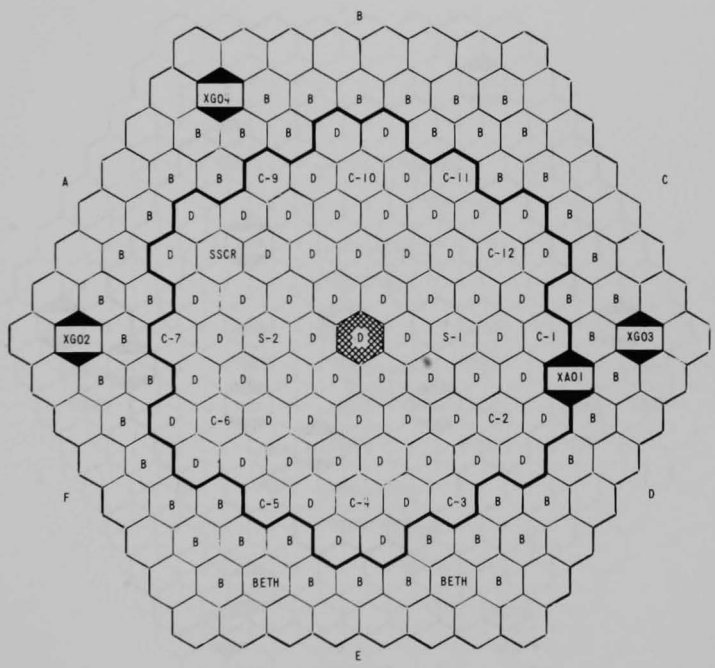

Fig. 3. Core-loading Pattern for Run 7. ANL Neg. No. ID-103-M5684.

TABLE III. Data for EBR-II Run 14 (80-subassembly core size)

Chronology	
Date started	1/10/66
Date ended	1/22/66
Number of days for run	12
Power Data	
(A) Cumulative MWd(t) at start of run	5050
(B) Cumulative MWd(t) at end of run	5570
MWd(t) generated during run (B-A)	520
Types of Subassemblies in Core	
Blanket	18
Core	43
Control rod	11
Safety rod	2
Experimental (rows 1-6)	5
Experimental Subassemblies in Row 7	3

Key to Types of Subassemblies Shown in Loading Diagram (Fig. 4)

B--Depleted Uranium
BETH--Beryllium Thimble
C--Control Rod
D--Driver Fuel
S--Safety Rod
SSCR--Stainless Steel Control Rod
X--Experimental Subassembly

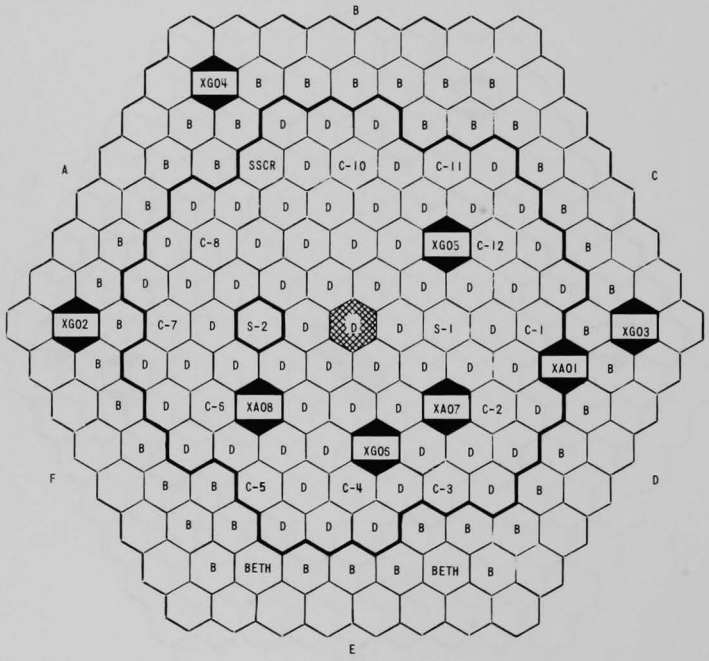

Fig. 4. Core-loading Pattern for Run 14. ANL Neg. No. ID-103-M5685.

TABLE IV. Data for EBR-II Run 29A (87-subassembly core size)

Chronology	
Date started	6/26/68
Date ended	7/5/68
Number of days for run	9
Power Data	
(A) Cumulative MWd(t) at start of run	17,984
(B) Cumulative MWd(t) at end of run	18,172
MWd(t) generated during run (B-A)	188
Types of Subasemblies in Core	
Blanket	23
Core	35
Control rod	11
Safety rod	2
Experimental (rows 1-6)	15
Experimental Subassemblies in Row 7	5

Key to Types of Subassemblies Shown in Loading Diagram (Fig. 5)

B--Depleted Uranium
BETH--Beryllium Thimble
C--Control Rod
D--Driver Fuel
OSC--Oscillator Rod
P--1/2 Driver Fuel and 1/2 Stainless Steel
R--Stainless Steel Reflector
S--Safety Rod
SSCR--Stainless Steel Control Rod
SST--Stainless Steel Thimble
X--Experimental Subassembly

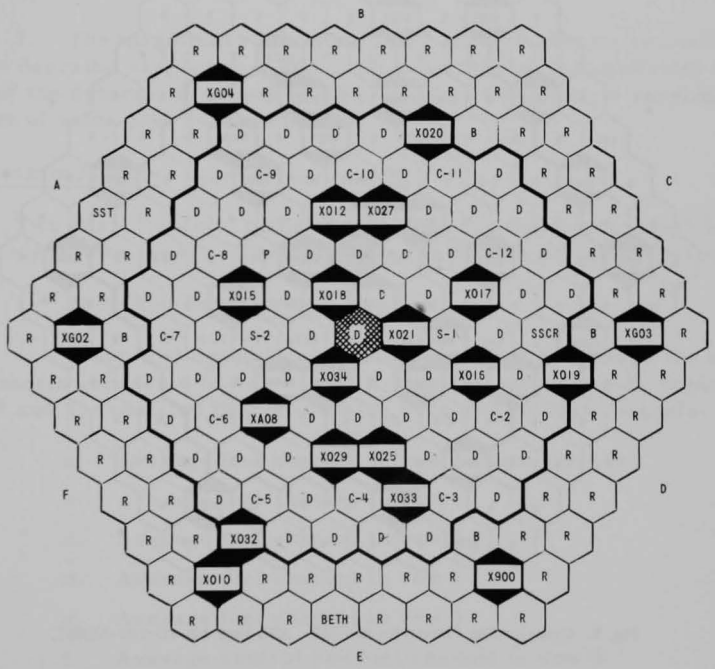

Fig. 5. Core-loading Pattern for Run 29A. ANL Neg No. ID-103-M5686.

TABLE V. Data for EBR-II Run 38B (90-subassembly core size)

Chronology	
Date started	10/3/69
Date ended	10/16/69
Number of days for run	13
Power Data	
(A) Cumulative MWd(t) at start of run	29,440
(B) Cumulative MWd(t) at end of run	30,040
MWd(t) generated during run (B-A)	600
Types of Subassemblies in Core	
Blanket	25
Core	32
Control rod	11
Safety rod	2
Experimental (rows 1-6)	19
Experimental Subassemblies in Row 7	10

Key to Types of Subassemblies Shown in Loading Diagram (Fig. 6)

B--Depleted Uranium
BETH--Beryllium Thimble
C--Control Rod
CF--Controlled-flow Subassembly
D--Driver Fuel
MK II--Mark-II Fuel
Ni--Nickel-corrosion Subassembly
P--1/2 Driver Fuel and 1/2 Stainless Steel
S--Safety Rod
70%--Driver Fuel Enriched to 70% ^{235}U
SSCR--Stainless Steel Control Rod
SST--Stainless Steel Thimble
X--Experimental Subassembly

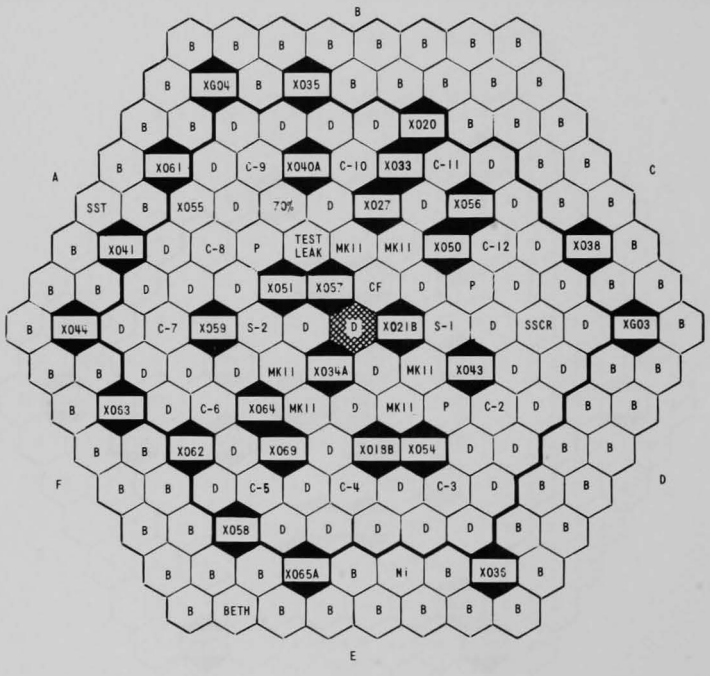

Fig. 6. Core-loading Pattern for Run 38B. ANL Neg. No. ID-103-M5687.

The irradiation experiments loaded into the EBR-II core have predominantly contained fuel elements of mixed plutonium and uranium oxide. Clearly the trend presented in Fig. 1 is upward, projecting an increased number of in-core experiments and therefore an increased number of oxide-fuel experiments.

III. DYNAMIC SIMULATION OF REACTOR-CORE LOADINGS

In the study of future EBR-II cores containing a varying complement of ceramic fuel elements and metallic driver-fuel elements, many assumptions must be made to allow a simulation of the dynamic behavior of the cores. These assumptions, along with the models and limitations, are briefly discussed below.

A. Assumptions

1. A reactor-core loading may be simulated by assuming that the peak-power-density and average-power-density driver and experimental fuel elements typify the core.

2. Space-independent kinetics are sufficient to describe the dynamic behavior of the EBR-II core during both normal and abnormal reactor-operating conditions.

3. The magnitudes of temperature-induced reactivity coefficients used to describe various past rod-drop experiments are applicable to the study of the dynamic response of EBR-II cores containing a varying complement of oxide-fuel subassemblies.

B. Dynamic Models

Two basic dynamic models were used in studies presented in the main body of this report. These models are briefly discussed below.

1. Rod-drop Experiments

A detailed dynamic simulation was used to analyze the rod-drop experiments conducted on various EBR-II cores. This model, depicted in Figs. 7 and 8, consisted of the following core and blanket channels:

a. Average fuel channel in row 1 (core center)

b. Average fuel channel in row 2

c. Average fuel channel in row 3

d. Average fuel channel in row 4

e. Average fuel channel in row 5

f. Average control rod fuel channel in row 5

g. Average fuel channel in row 6

h. Average fuel channel in inner-blanket region.

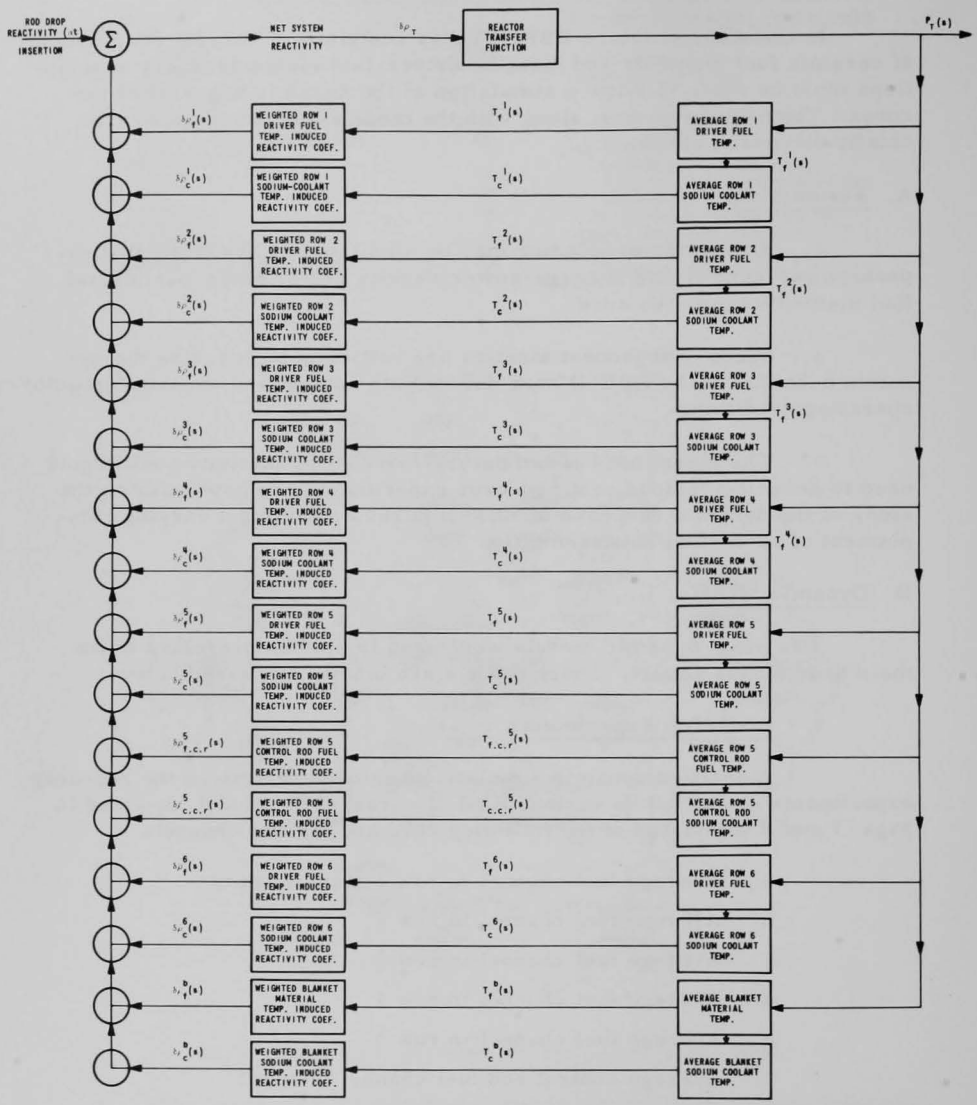

Fig. 7. Feedback Network for Simulating the Closed-loop Behavior of EBR-II during Rod-drop Experiments. ANL Neg. No. ID-103-M5688.

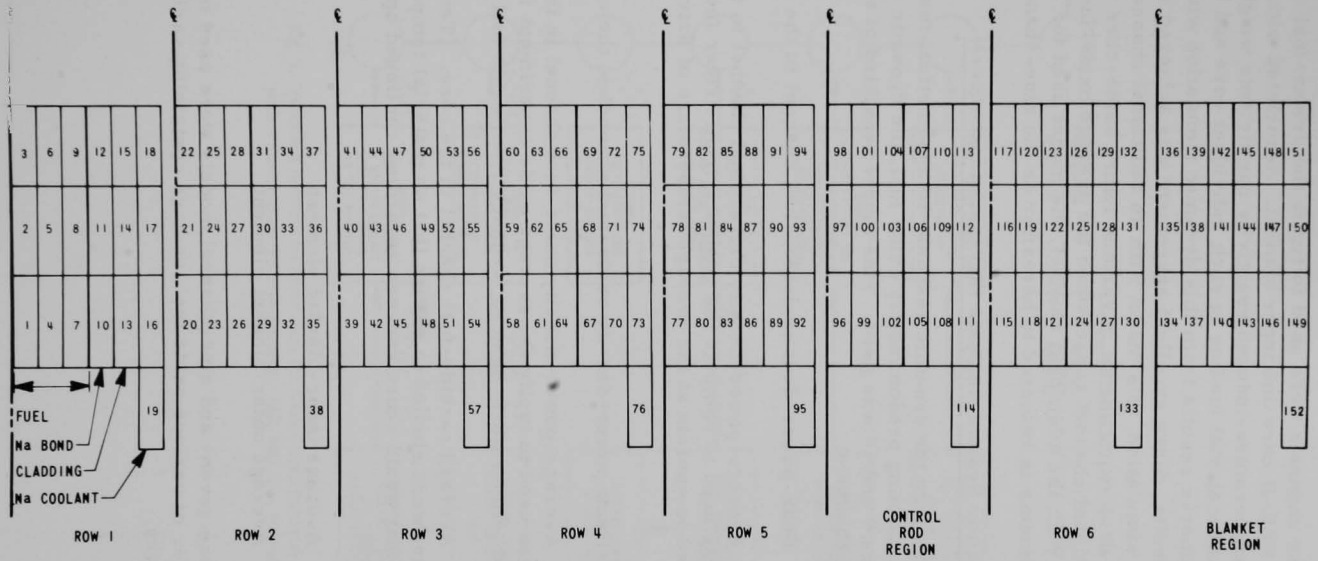

Fig. 8. Eight-channel Representation of EBR-II Core and Blanket for Feedback Modeling for Rod-drop Experiments. ANL Neg. No. ID-103-M5689.

These channels were used to typify the driver-fuel and blanket elements in the EBR-II core and inner blanket. Associated with these channels were temperature-induced reactivity coefficients weighed according to position and material loading in each individual core and blanket row. Reference 4 compares results from this dynamic simulation with earlier experimental results. Since excellent agreement was achieved with this type of dynamic simulation, this model with an additional channel was used to simulate rod-drop experiments in various future oxide-core configurations. The additional channel represented the average oxide-fuel experiment in row 5. With the additional channel, the model used for study of rod-drop experiments is referred to hereafter as the nine-channel model.

2. Dynamic System Analysis (seven-channel model)

To analyze the dynamic response to hypothetical malfunctions in EBR-II cores containing predominantly oxide fuel, the dynamic simulation presented in Figs. 9 and 10 was used. This model consisted of the following fuel and blanket channels:

a. Peak-power-density driver-fuel channel in the core.

b. Average-power-density driver-fuel channel in the core. (This channel was used to compute the feedback from driver fuel in the core and was specified to operate at the average temperature of driver fuel in the core.)

c. Peak-power-density oxide-fuel channel in the core.

d. Average-power-density oxide-fuel channel in the core. (This channel was used to typify the average oxide experiment in the core and the expected temperature-induced feedback from oxide fuel.)

e. Average carbide-fuel channel in the core. (Temperatures from this channel were studied to ensure that no material temperature exceeded a value that would cause concern regarding continued operation of the EBR-II core.)

f. Average inner-blanket element.

g. Average outer-blanket element.

These seven- and nine-channel models were used to study the dynamic behavior of various oxide fuel loadings containing various assumed feedback networks.

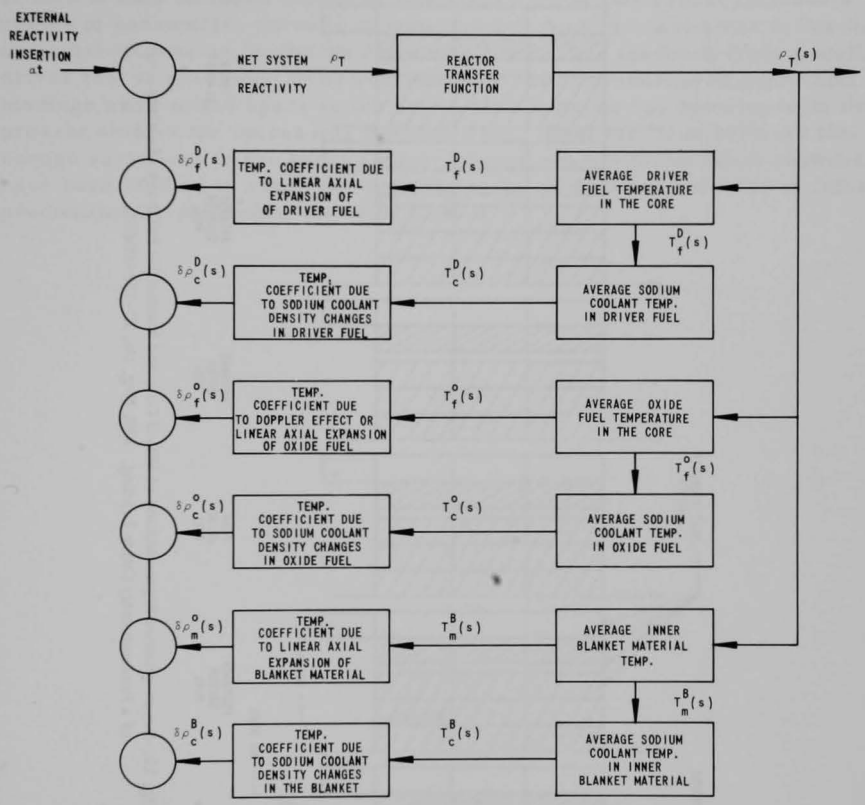

Fig. 9. Feedback Network for Simulating the Closed-loop Behavior of EBR-II with a Predominantly Oxide Loading. ANL Neg. No. ID-103-M5690.

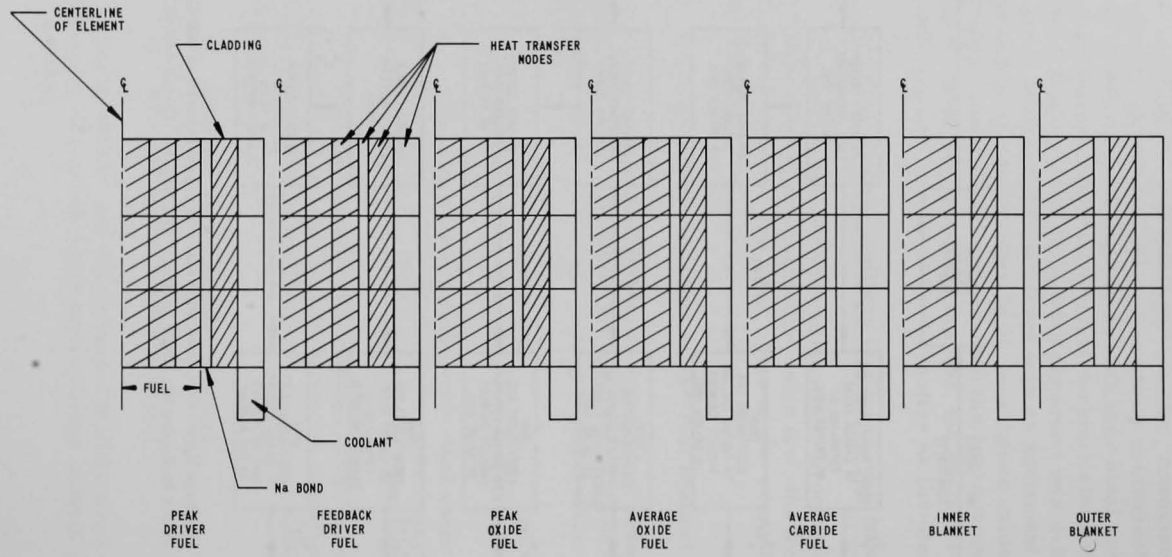

Fig. 10. Seven-channel Representation of EBR-II Core and Blanket for Feedback Modeling of a Predominantly Oxide Loading. ANL Neg. No. ID-103-M5691.

C. Limitations

The limitations of this study are inherent in the assumptions made to survey the dynamic behavior of predominantly oxide cores. The principal limitation has to do with the assumptions that must be made about temperature-induced reactivity-feedback networks in oxide cores. Because of lack of data on these networks, the main body of this report includes a series of parametric surveys of expected and possible variations in Doppler and axial-expansion feedbacks from oxide fuel. The feedback from metallic driver fuel is presumed to be reduced as a result of increased oxide-fuel loadings and limited space in the core. No allowance has been made in the present studies for increasing the core size. However, it is believed that enough variations in the temperature-induced reactivity-feedback networks have been studied to cover the possible range of dynamic behavior of future predominantly oxide-fuel cores in EBR-II.

IV. FUNDAMENTAL DYNAMIC BEHAVIOR OF OXIDE AND METALLIC FUEL ELEMENTS

Oxide and metallic fuel elements are basically different in dynamic behavior because of their physical properties. The dynamic behavior of metallic driver-fuel elements is typical of conductors having a high thermal conductivity, as opposed to oxide elements, which have the characteristics of an insulator with a low thermal conductivity. The effects of these physical properties on the dynamic behavior of fuel elements are studied in the following subsections. The seven-channel model described in the previous section was used in this portion of the study. The assumed operating characteristics of each channel are presented in Table VI. The values in the table assume a reactor power level of 62.5 MWt.

TABLE VI. Seven-channel Model Used in the Dynamic System Analysis of Predominantly Oxide Fuel Loadings in EBR-II

Channel Number	Simulation	Reactor Power = 62.5 MWt	
		Power, Btu/sec	Flow, lb/sec
1	Peak driver-fuel element	9.832	0.1490
2	Feedback driver-fuel element	7.548	0.0980
3	Peak oxide-fuel element	18.00	0.210
4	Feedback oxide-fuel element	13.60	0.1550
5	Average carbide-fuel element	22.70	0.3140
6	Average inner-blanket element	12.70	0.1280
7	Average outer-blanket element	1.945	0.0362

A. Physical Properties of Fuel Elements

Figure 11 shows the measured thermal conductivity of uranium-5 wt % fissium and PuO_2-UO_2 fuel as a function of temperature. As indicated, the thermal conductivity of uranium-5 wt % fissium is at least an order of magnitude higher than that for the PuO_2-UO_2 fuel over the normal operating range of each fuel type. The initial effect of this difference in

thermal conductivity would appear as a higher rate of heat transfer from a metallic element as compared to an oxide element. Figure 12 shows the specific heat of uranium-5 wt % fissium and PuO_2-UO_2 in the normal operation range of each type of fuel. The effect of this property would be to require more heat input to raise a given amount of oxide fuel through a given temperature range. To study, in a general way, the effect of these properties separately on dynamic behavior of metallic and oxide fuel, the physical properties were initially assumed to be those presented in Table VII. Although these physical properties are normally a function of temperature over the radius of the fuel pin in the dynamic-channel simulation, they were assumed not to vary with radius in this survey. The properties of metallic driver fuel were then held constant in the following studies and only the oxide-fuel properties were varied.

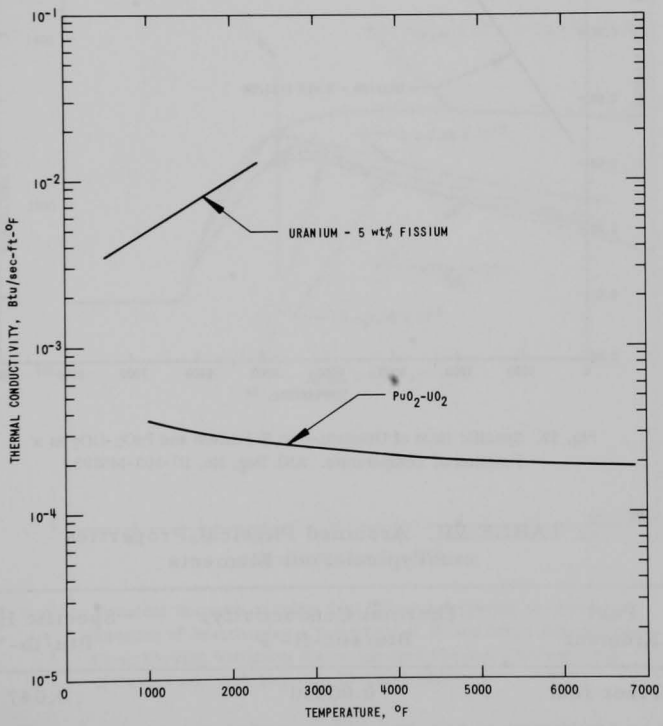

Fig. 11. Thermal Conductivity of Uranium-5 wt % Fissium and PuO_2-UO_2 as a Function of Temperature. ANL Neg. No. ID-103-M5692.

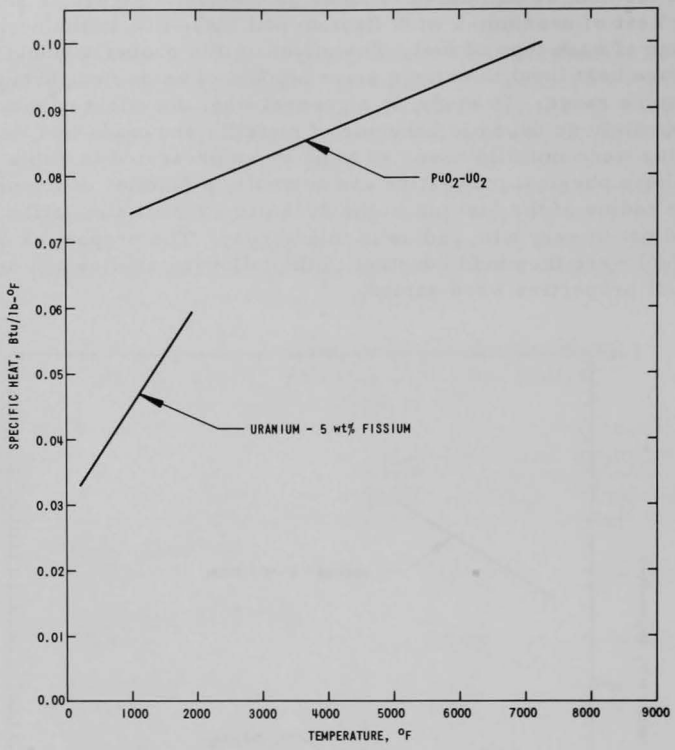

Fig. 12. Specific Heat of Uranium-5 wt % Fissium and PuO_2-UO_2 as a Function of Temperature. ANL Neg. No. ID-103-M5693.

TABLE VII. Assumed Physical Properties of Typical Fuel Elements

Fuel Element	Thermal Conductivity, Btu/sec-ft-°F	Specific Heat, Btu/lb-°F
Driver fuel	0.00530	0.047
Oxide fuel	0.00036	0.082

B. General Dynamic Behavior

Figure 13 presents the transient response of oxide fuel following an assumed insertion of reactivity at a ramp rate of 5$/sec in a just-critical core. A wide range of variations in the thermal conductivity of oxide fuel is included, but the specific heat is held constant. The figure shows that for the assumed variations in thermal conductivity, the temperature profiles vary widely.

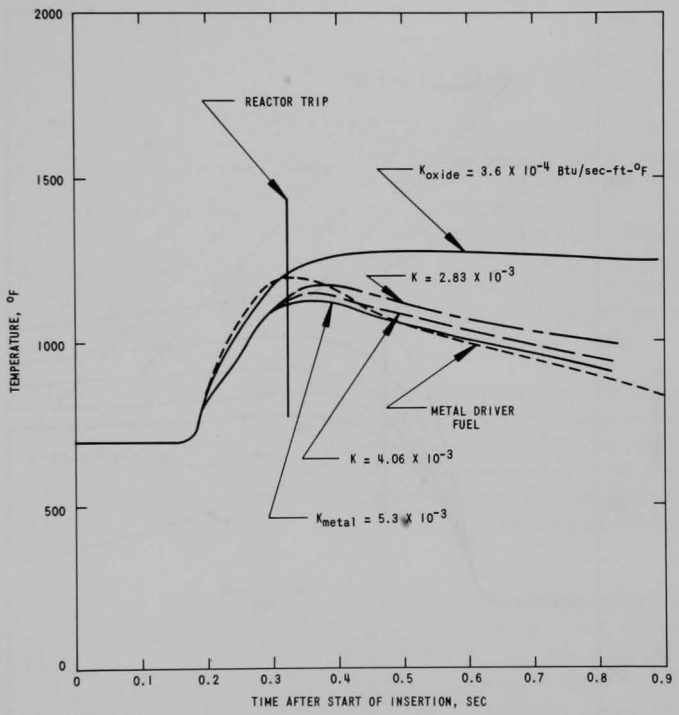

Fig. 13. Transient Response of Oxide Fuel Elements following an Accidental Insertion of Reactivity at a Ramp Rate of 5$/sec into a Just-critical Core, Showing Variations due to Assumed Thermal Conductivities of Oxide Fuel. ANL Neg. No. ID-103-M5694.

Following a reactor trip at 0.325 sec, the temperature of the metallic driver-fuel element decreases rapidly to isothermal conditions of 700°F. Meanwhile, the oxide element in the top curve maintains its temperature because of its extremely long time constant. The time constant of metallic driver-fuel elements is approximately 0.3 sec, as opposed to 4.0 sec for the oxide fuel element. This difference in time constant is principally due to the difference in thermal conductivity.

Figure 14 also shows the transient response of oxide fuel following an accidental insertion of reactivity at a ramp rate of 5$/sec in a just-critical core, but only variations in oxide-fuel specific heat are included. The thermal conductivity is held constant at the values listed in Table VII. Here, again, the driver-fuel temperature following a trip at 0.325 sec promptly decays to its isothermal value of 700°F. As the specific heat of the oxide is lowered to approach the specific heat of the metal, the oxide element shows an increased heat rate prior to the reactor trip. Following

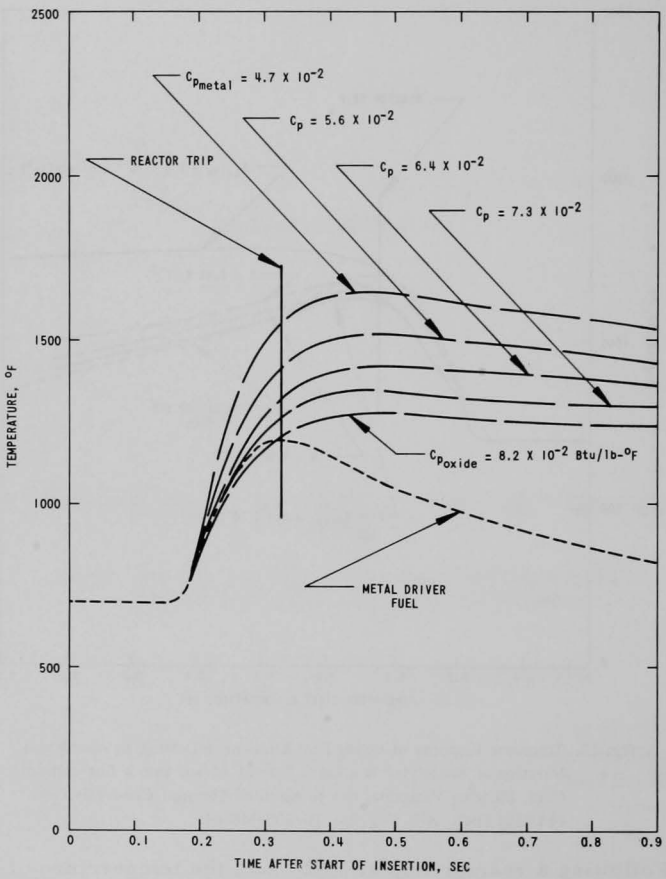

Fig. 14. Transient Response of Oxide Fuel Elements following an Accidental Insertion of Reactivity at a Ramp Rate of 5$/sec into a Just-critical Core, Showing Variations due to Assumed Specific Heats of Oxide Fuel. ANL Neg. No. ID-103-M5695.

the trip, the low thermal conductivity of the oxide causes all temperatures to remain at a higher level than the transient temperatures of the driver-fuel element for the same time interval.

Figures 13 and 14 demonstrate that the physical properties of oxide fuel will affect the temperature of the oxide fuel element, both during a reactor transient and after a reactor trip; and this behavior is governed mainly by the oxide-fuel thermal conductivity. The influence of this phenomenon on the dynamic behavior of oxide fuel elements is reviewed in greater detail in the following sections.

C. The Effect of Thermal Conductivity on Dynamic Response

To investigate the fuel behavior in further detail, the startup transient behavior of oxide-fuel elements with various assumed physical properties was studied, using hypothetical reactivity insertions spanning the range from 0.01 to 10$/sec. In the first series of cases, the measured physical properties of the metallic and oxide fuel elements were used to establish a base case. Figures 15-18 present the transient characteristics of the central heat-transfer node of the peak oxide and metallic fuel elements following various reactivity insertions. All of these cases assume the full primary-coolant flow.

The figures show that as the reactivity insertion decreases, the peak oxide temperature rises appreciably above the peak metallic-fuel temperature. This behavior is principally due to the lower thermal conductivity of the oxide elements as compared to metallic elements. In all cases, the reactor is assumed to be tripped at the point of metallic-driver-fuel melting of 1834°F, and the figures show the decrease in temperatures following the trip.

These results are summarized in Fig. 19, which shows the maximum fuel temperatures for various reactivity ramp rates, assuming measured physical properties. Under conditions of full flow, the peak-oxide center node will be the first point of melting in the reactor core for reactivity ramps of less than 0.1$/sec. For reactivity ramp rates of greater than 0.1$/sec, melting of the peak-metal central node will occur prior to oxide melting. The results show that the first point of melting in an EBR-II core containing experimental oxide elements is dependent on the reactivity ramp rate assumed to be present during a component malfunction. These results will be used later in analyzing control- and safety-rod malfunctions.

To further study the effect of thermal conductivity on the dynamic characteristics of oxide elements, the assumption was made that the thermal conductivity of the oxide was equal to that of the metal, and the measured specific heats of the metal and the oxide were used. Figures 20-23 present peak fuel temperatures following the inadvertent insertion of

reactivity at ramp rates varying from 10 to 0.1$/sec, under conditions of a just-critical core with full primary flow. (As above, the reactor is assumed to be tripped at the point of metallic-driver-fuel melting of 1834°F.) The figures show that the peak temperatures in the oxide and metallic elements are close together for all reactivity insertions.

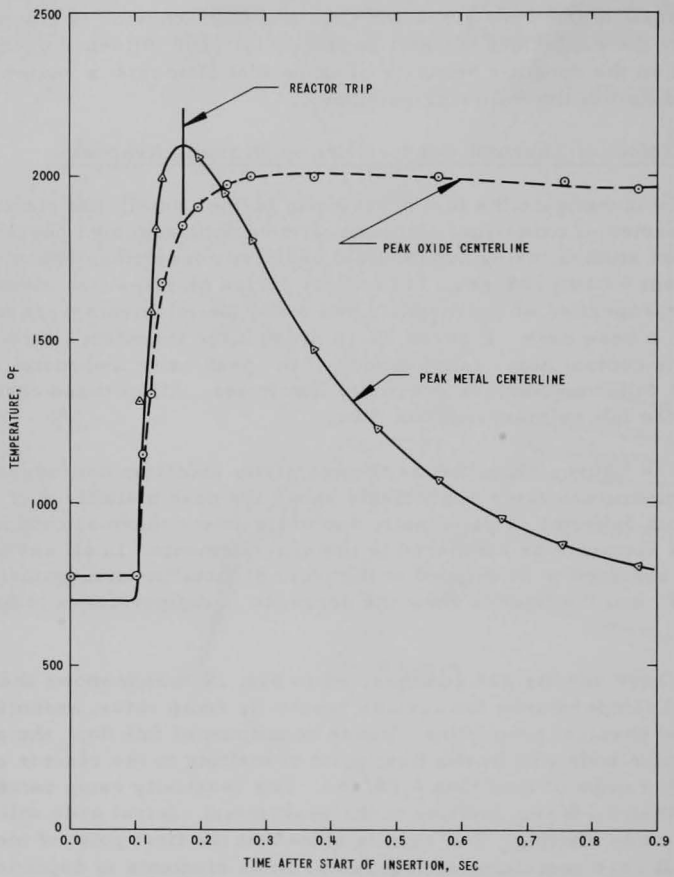

Fig. 15. Peak Fuel Temperatures following an Inadvertent Insertion of Reactivity at a Ramp Rate of 10$/sec into a Just-critical Core under Conditions of Full Primary-coolant Flow, Using Measured k and C_p for Oxide Fuel. ANL Neg. No. ID-103-M5696.

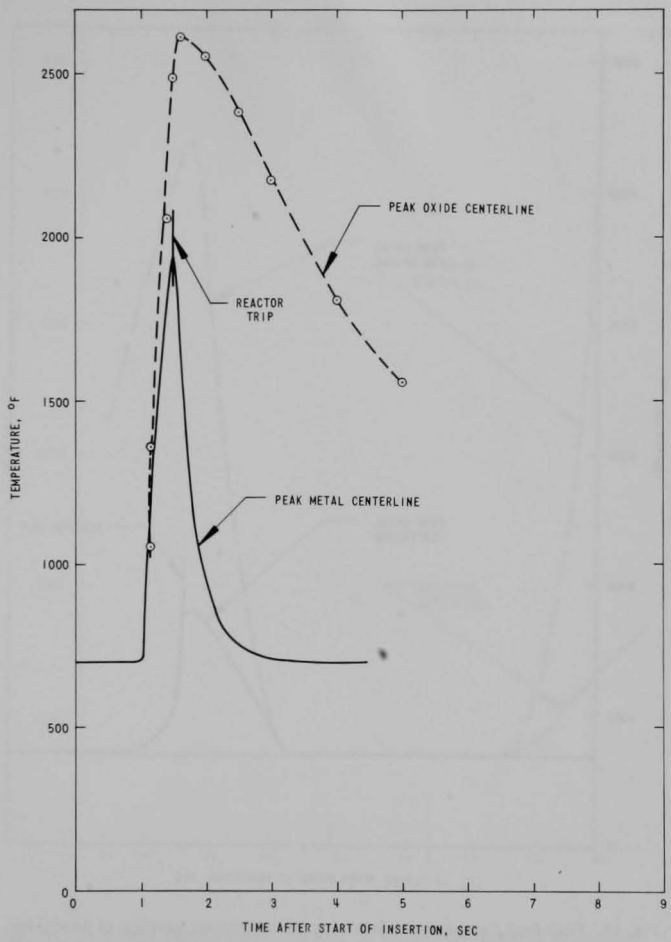

Fig. 16. Peak Fuel Temperatures following an Inadvertent Insertion of Reactivity at a Ramp Rate of 1.0$/sec into a Just-critical Core under Conditions of Full Primary-coolant Flow, Using Measured k and C_p for Oxide Fuel. ANL Neg. No. ID-103-M5697.

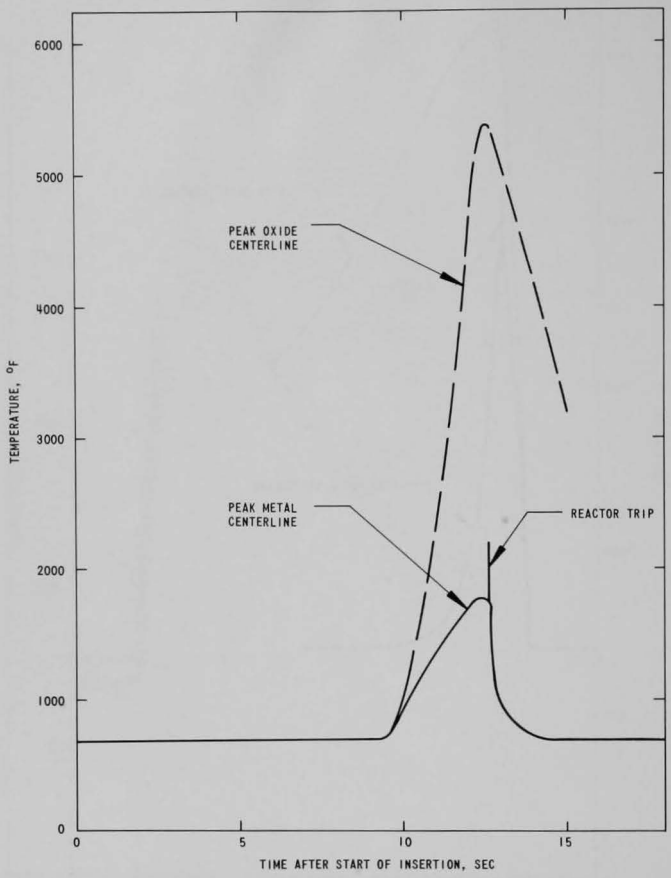

Fig. 17. Peak Fuel Temperatures following an Inadvertent Insertion of Reactivity at a Ramp Rate of 0.1$/sec into a Just-critical Core under Conditions of Full Primary-coolant Flow, Using Measured k and C_p for Oxide Fuel. ANL Neg. No. ID-103-M5698.

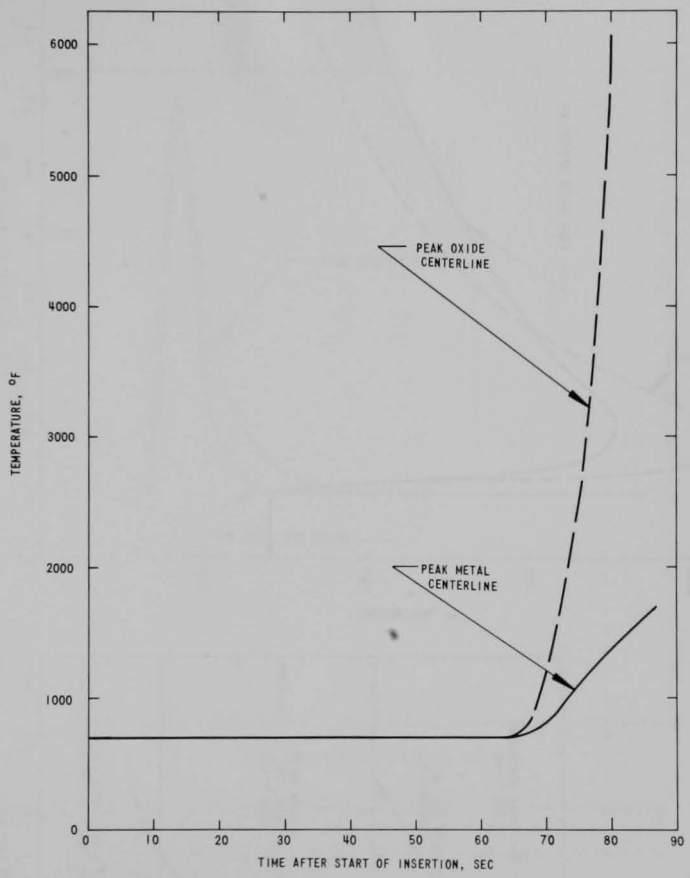

Fig. 18. Peak Fuel Temperatures following an Inadvertent Insertion of Reactivity at a Ramp Rate of 0.01$/sec into a Just-critical Core under Conditions of Full Primary-coolant Flow, Using Measured k and C_p for Oxide Fuel. ANL Neg. No. ID-103-M5699.

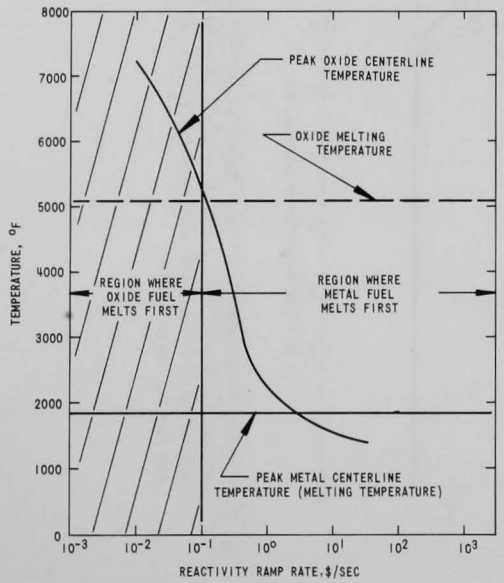

Fig. 19. Peak Fuel Temperatures for Various Reactivity Ramp Rates, Using Measured k and C_p for Oxide Fuel. ANL Neg. No. ID-103-M5700.

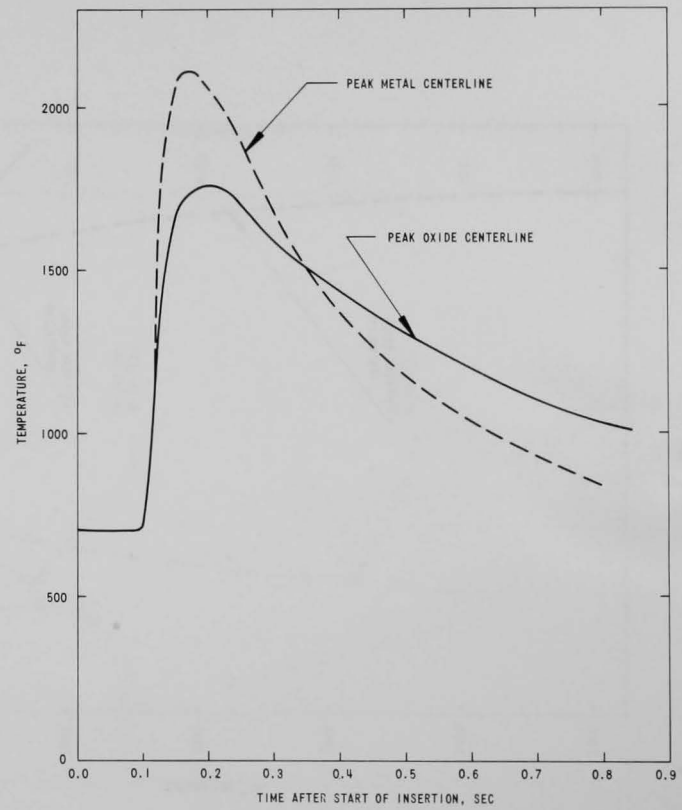

Fig. 20. Peak Fuel Temperatures following an Inadvertent Insertion of Reactivity at a Ramp Rate of 10$/sec into a Just-critical Core under Conditions of Full Primary-coolant Flow, Using Measured C_p and Oxide k = Metal k. ANL Neg. No. ID-103-M5701.

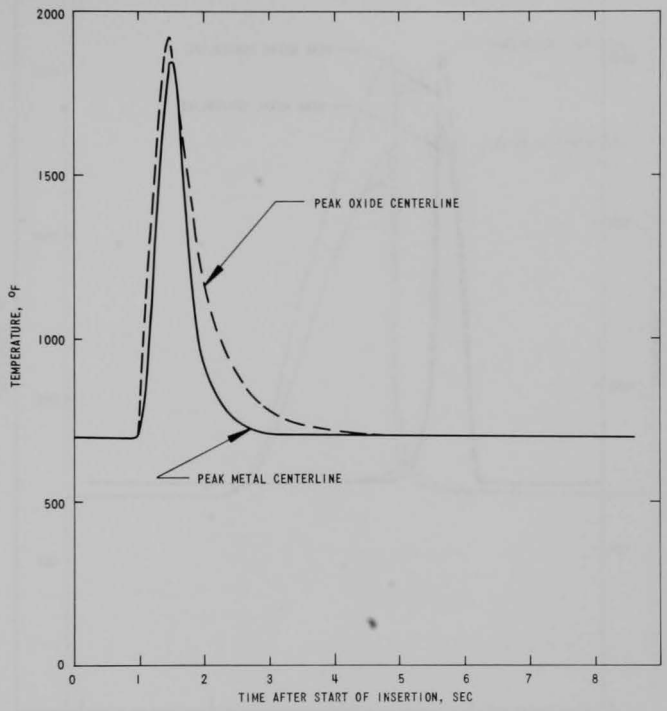

Fig. 21. Peak Fuel Temperatures following an Inadvertent Insertion of Reactivity at a Ramp Rate of 1.0$/sec into a Just-critical Core under Conditions of Full Primary-coolant Flow, Using Measured C_p and Oxide k = Metal k. ANL Neg. No. ID-103-M5702.

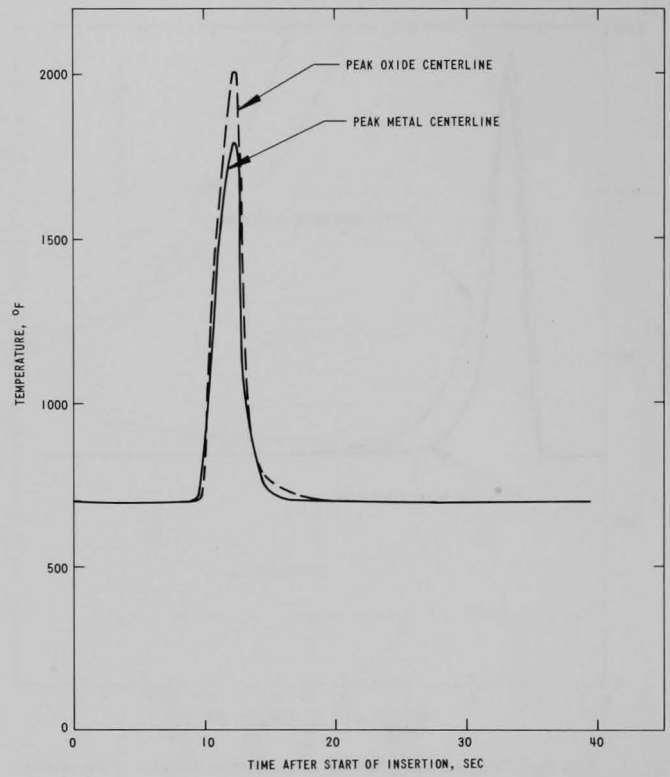

Fig. 22. Peak Fuel Temperatures following an Inadvertent Insertion of Reactivity at a Ramp Rate of 0.1$/sec into a Just-critical Core under Conditions of Full Primary-coolant Flow, Using Measured C_p and Oxide k = Metal k. ANL Neg. No. ID-103-M5703.

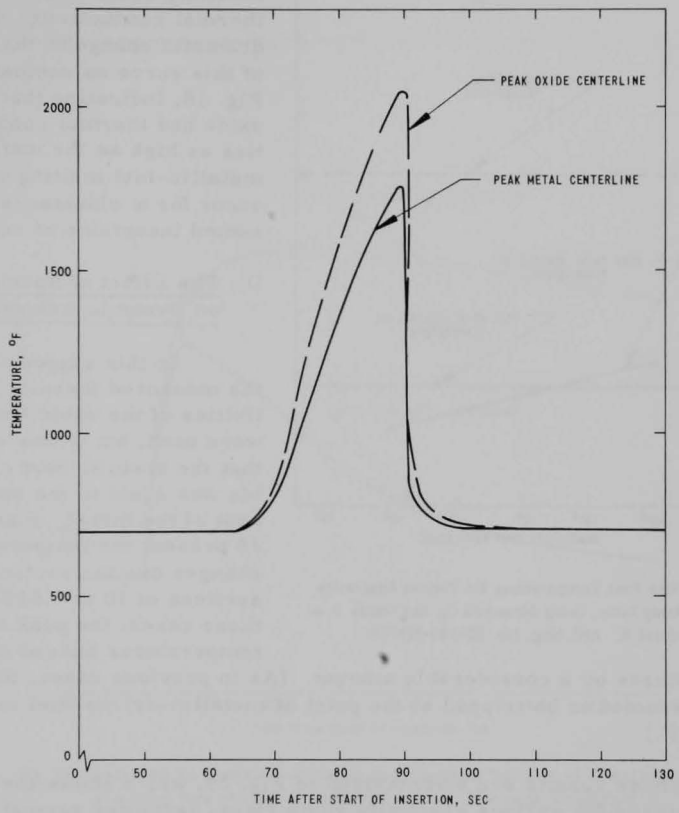

Fig. 23. Peak Fuel Temperatures following an Inadvertent Insertion of Reactivity at a Ramp Rate of 0.01$/sec into a Just-critical Core under Conditions of Full Primary-coolant Flow, Using Measured C_p and Oxide k = Metal k. ANL Neg. No. ID-103-M5704.

These results are summarized in Fig. 24, which indicates the fuel temperatures for various reactivity ramp rates, assuming normal specific heat, but the oxide thermal conductivity equal to the metallic thermal conductivity. Note the dramatic change in the shape of this curve as compared to Fig. 18, indicating that if the oxide had thermal conductivities as high as the metal, only metallic-fuel melting would occur for a wide range of assumed insertions of reactivity.

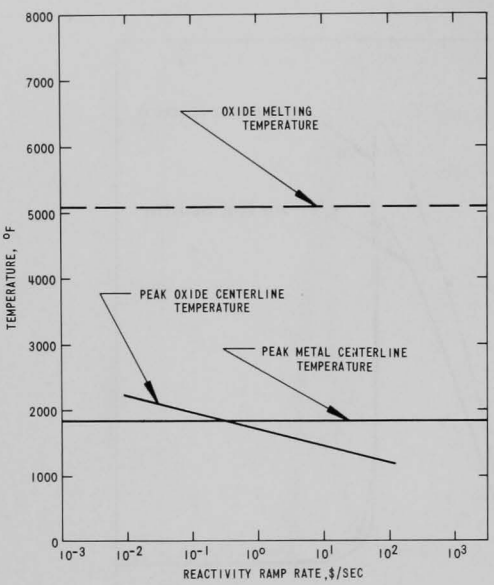

Fig. 24. Peak Fuel Temperatures for Various Reactivity Ramp Rates, Using Measured C_p and Oxide k = Metal k. ANL Neg. No. ID-103-M5705.

D. The Effect of Specific Heat on Dynamic Response

In this series of cases, the measured thermal conductivities of the oxide and metal were used, but it was assumed that the specific heat of the oxide was equal to the specific heat of the metal. Figures 25-28 present the temperature changes due to reactivity insertions of 10 to 0.01$/sec. In these cases, the peak oxide temperatures exceed the metal temperatures by a considerable amount. (As in previous cases, the reactor is assumed to be tripped at the point of metallic-driver-fuel melting of 1834°F.)

These results are summarized in Fig. 29, which shows the fuel temperatures for various reactivity ramp rates, assuming normal thermal conductivity, but with the specific heat of the oxide equal to the specific heat of the metal. Note that there is a slight shift in the point at which oxide melts first. This point now occurs at a reactivity ramp rate of less than 0.4$/sec, indicating that decreases in specific heat only aggravate oxide-fuel melting by increasing the heating rate for the same assumed heat-transfer capability.

The effects of thermal conductivity and specific heat on the transient behavior of oxide elements will be used in the following sections to analyze various combinations of operating conditions in which the dynamic behavior of oxide and metallic elements plays a prominent role.

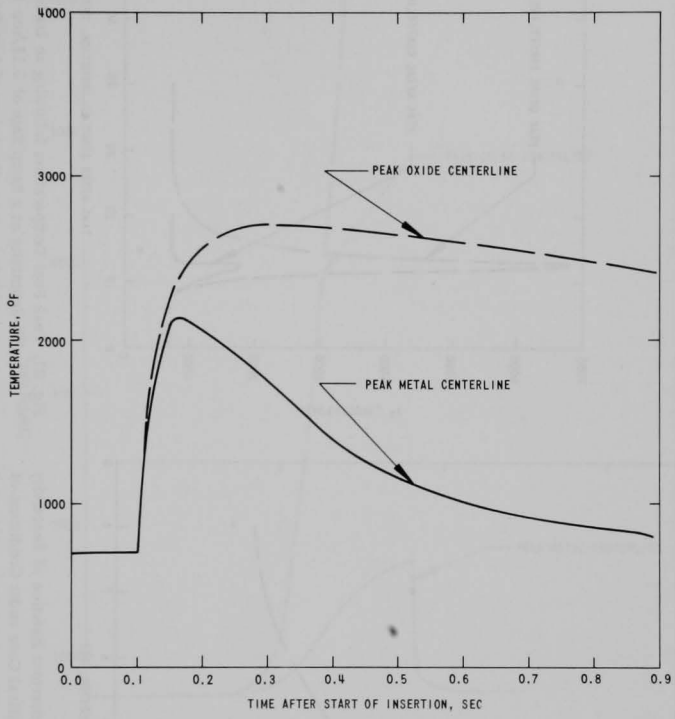

Fig. 25. Peak Fuel Temperatures following an Inadvertent Insertion of Reactivity at a Ramp Rate of 10$/sec into a Just-critical Core under Conditions of Full Primary-coolant Flow, Using Measured k and Oxide C_p = Metal C_p. ANL Neg. No. ID-103-M5706.

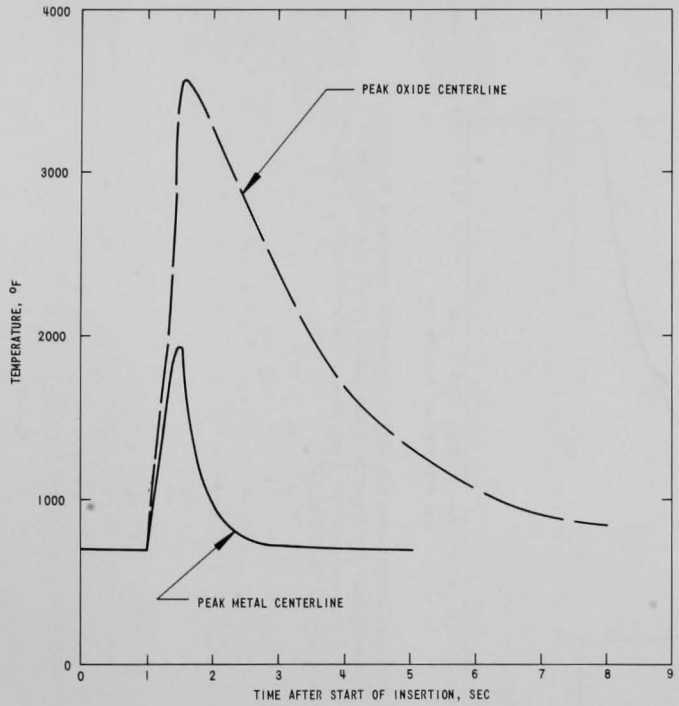

Fig. 26. Peak Fuel Temperatures following an Inadvertent Insertion of Reactivity at a Ramp Rate of 1.0$/sec into a Just-critical Core under Conditions of Full Primary-coolant Flow, Using Measured k and Oxide C_p = Metal C_p. ANL Neg. No. ID-103-M5707.

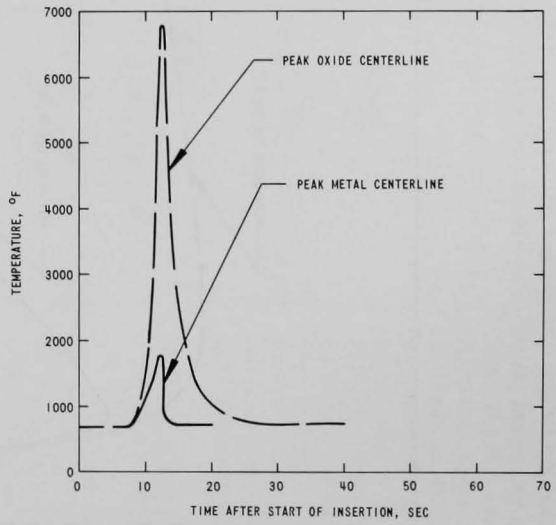

Fig. 27. Peak Fuel Temperatures following an Inadvertent Insertion of Reactivity at a Ramp Rate of 0.1$/sec into a Just-critical Core under Conditions of Full Primary-coolant Flow, Using Measured k and Oxide C_p = Metal C_p. ANL Neg. No. ID-103-M5708.

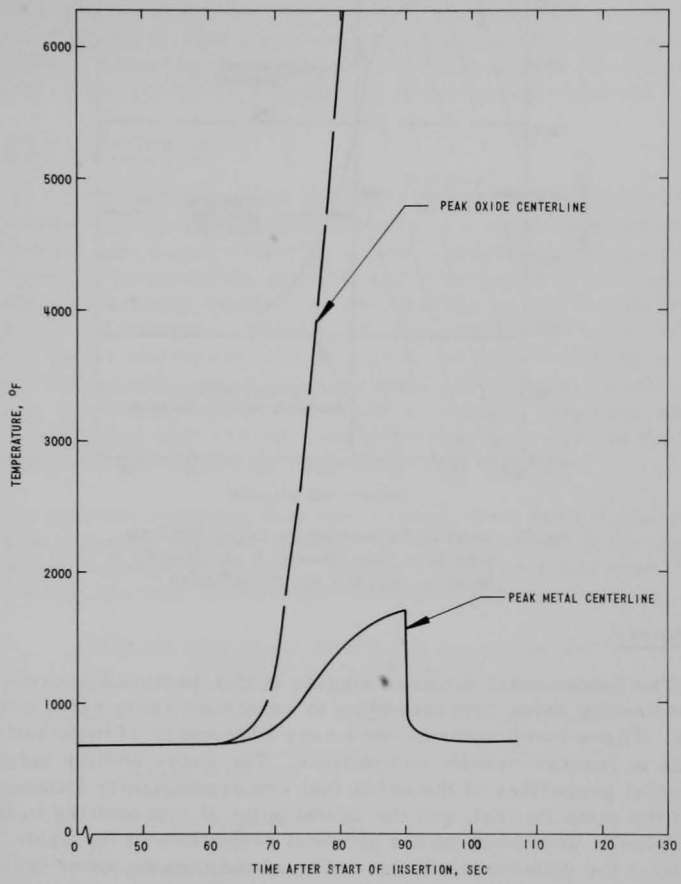

Fig. 28. Peak Fuel Temperatures following an Inadvertent Insertion of Reactivity at a Ramp Rate of 0.01$/sec into a Just-critical Core under Conditions of Full Primary-coolant Flow, Using Measured k and Oxide C_p = Metal C_p. ANL Neg. No. ID-103-M5709.

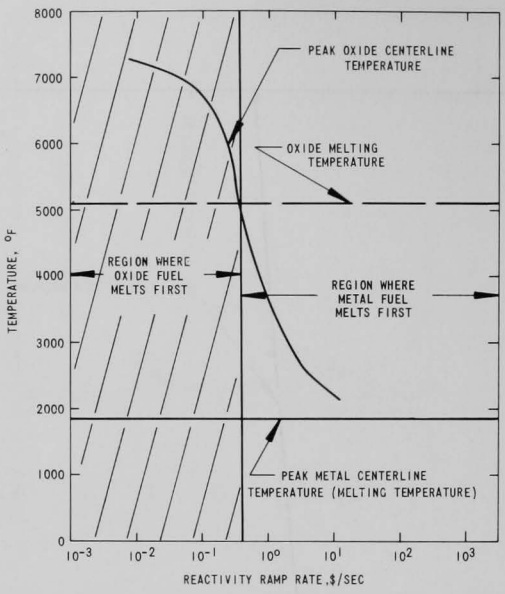

Fig. 29. Peak Fuel Temperatures for Various Reactivity Ramp Rates, Using Measured k and Oxide C_p = Metal C_p. ANL Neg. No. ID-103-M5710.

E. Summary

The fundamental dynamic studies in this section have covered a range of heating rates corresponding to reactivity ramp rates of 0.01 to 10$/sec. These ramp rates cover a very wide range of hypothetical malfunctions in reactor-system components. The above studies indicate that the physical properties of the oxide fuel are dramatically different from those of the metallic fuel, and the initial point of fuel melting in the EBR-II core is heavily dependent on the physical properties of the oxide. The most dramatic of the differences is the order-of-magnitude-lower thermal conductivity of the oxide as compared to the metallic driver fuel. The effect of this decreased thermal conductivity in future cores predominantly loaded with oxide fuel will be analyzed in the following sections.

V. DYNAMIC BEHAVIOR DURING NORMAL REACTOR OPERATIONS

Two types of normal reactor operations are studied in this section: (1) reactor stability tests involving rod-drop experiments, and (2) reactor conditions initiating an automatic reactor trip. Only that portion of the power transient following the trip is examined, to assess the differences in the decay of temperatures in oxide and metallic fuel elements.

A. Rod-drop Experiments

The nine-channel dynamic simulation described in Section III was used to study a variety of feedback networks to assess the characteristics of the rod-drop data acquired during normal experiments on the reactor plant. Table VIII presents the physical characteristics of each channel. All rod-drop-experiment studies are for 50 MWt, so that trends from measured data may be assessed. Figure 30 presents a typical set of data relating decrease in power and increase in reactivity feedback following a rod drop. This figure represents recent rod-drop tests conducted at 50 MWt using the present low-worth drop rod (whose worth is 0.011$). This base case will be used for comparison with various conditions that may exist as the EBR-II core is loaded with more and more ceramic fuel elements.

One possible condition that may prevail, if no design efforts are made to introduce a prompt negative feedback in the oxide fuel, is the worse case of no feedback from the oxide fuel. Figure 31 presents this case, in which it is assumed that the only temperature-induced reactivity feedback in the core

TABLE VIII. Nine-channel Model Used in Dynamic Simulation of EBR-II Rod-drop Experiments

Channel No.	Simulation	Reactor Power = 50 MWt	
		Power, Btu/sec	Flow, lb/sec
1	Average driver-fuel element in row 1	8.2438	0.2107
2	Average driver-fuel element in row 2	8.1552	0.1131
3	Average driver-fuel element in row 3	6.7561	0.1854
4	Average driver-fuel element in row 4	7.3374	0.1359
5	Average driver-fuel element in row 5	6.5508	0.1151
6	Average fuel element in control rods (row 5)	6.7786	0.0866
7	Average driver-fuel element in row 6	5.3778	0.0993
8	Average blanket element in row 7	3.9323	0.1429
9	Average oxide-fuel element in row 5	9.8715	0.2421

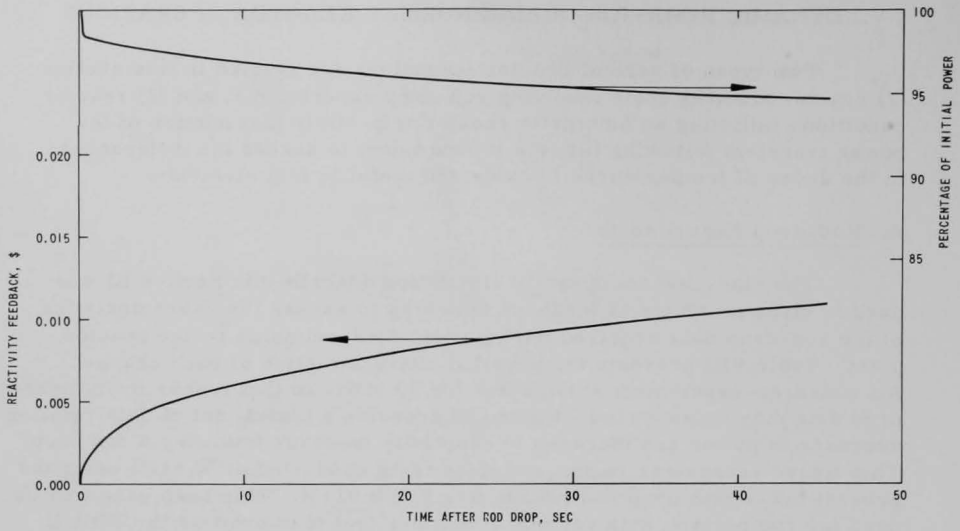

Fig. 30. Power and Reactivity Feedback following a Rod-drop Experiment at 50 MWt in a Typical Present Core Loading, with Only Driver-fuel and Sodium-coolant Feedback. ANL Neg. No. ID-103-M5711.

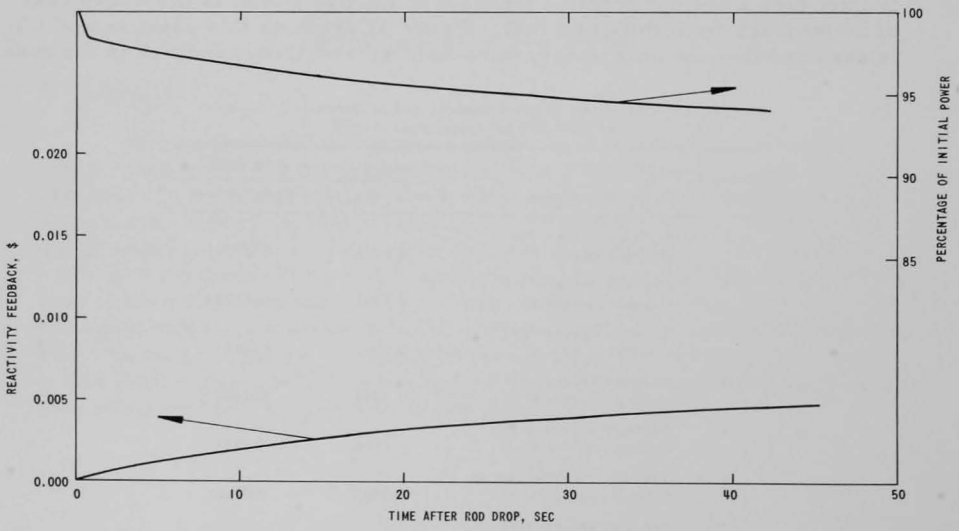

Fig. 31. Power and Reactivity Feedback following a Rod-drop Experiment at 50 MWt in a Predominantly Oxide-fuel Core, with Only Sodium-coolant Feedback. ANL Neg. No. ID-103-M5712.

is from the sodium coolant. The results are what would be expected if there were no feedback from the oxide fuel and should not be a surprise. Initial inspection of Fig. 31 could imply increased positive feedback, decreasing the overall negative feedback; however, the analysis indicates that if only sodium feedback were present, the type of results shown in the figure would be expected.

Possibly, with a fresh, heavily loaded core of oxide fuel elements, the reactivity coefficient due to linear axial expansion of the oxide could be appreciable. In Fig. 32 it is assumed that the reactivity coefficient due to linear axial expansion of the oxide fuel is equal to 80% of the reactivity coefficient for axial expansion of metallic fuel. As indicated, an increased reactivity feedback would be obtained in the rod-drop experiment, indicating an increase in the negative component of the prompt feedback in the reactor. These results would be expected if there were fuel expansion in fresh oxide-fuel elements.

Although fuel expansion might be present in fresh oxide fuel, it is expected, from the experience at the Rapsodie reactor in France, that the expansion would decrease as a function of irradiation time. If we now reduce the assumed reactivity coefficient due to oxide-fuel expansion to 40% of the coefficient for metallic driver fuel, the feedback curves will decrease as a function of time, as shown in Fig. 33. This result is to be expected if irradiation produces a gradual change in the temperature-induced reactivity coefficient due to axial expansion in the oxide fuel.

It is entirely possible that with increased oxide loadings, a Doppler coefficient may be present in the oxide fuel. If this is the case, Fig. 34 shows the kind of reactivity feedback that would be measured during the rod-drop experiments. The figure shows the reactivity feedbacks for a reactor core having a Doppler constant of $T\,\partial k/\partial T = -0.001$. This curve is similar to that for the base case, demonstrating that with a Doppler constant of -0.001 and a constant sodium-coolant temperature coefficient, this oxide core would have a dynamic behavior similar to that of the reference core with axial expansion of metallic driver fuel and normal sodium-density changes. Therefore, for a Doppler constant of -0.001, we would see no differences in rod-drop experiments in this oxide-fueled core as compared to earlier cases with only metallic driver fuel.

The last case considered assumes that the axial expansion of oxide fuel is equal to the axial expansion of metallic fuel, and the normal sodium-density changes are present. As Fig. 35 shows, there will be an appreciable reactivity feedback during a rod-drop experiment, and this is to be expected if there is an equal amount of fuel expansion in fresh oxide and metallic fuel. These results are summarized in Table IX, which compares rod-drop experiments assuming several different types of reactivity-feedback sources. All data are compared at the end of 40 sec after the rod drop. As the table

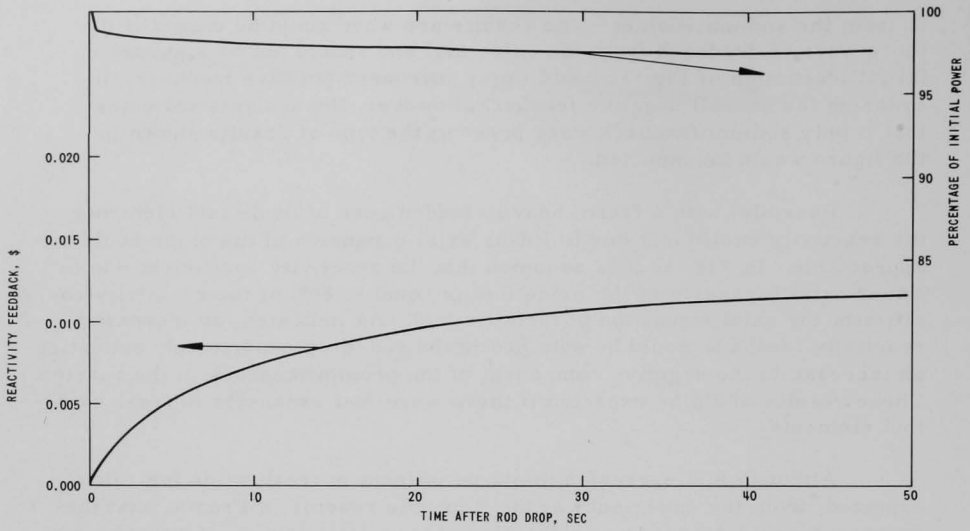

Fig. 32. Power and Reactivity Feedback following a Rod-drop Experiment at 50 MWt in a Predominantly Oxide-fuel Core, Assuming Feedback from Oxide-fuel Axial Expansion and Sodium-density Changes. ANL Neg. No. ID-103-M5713.

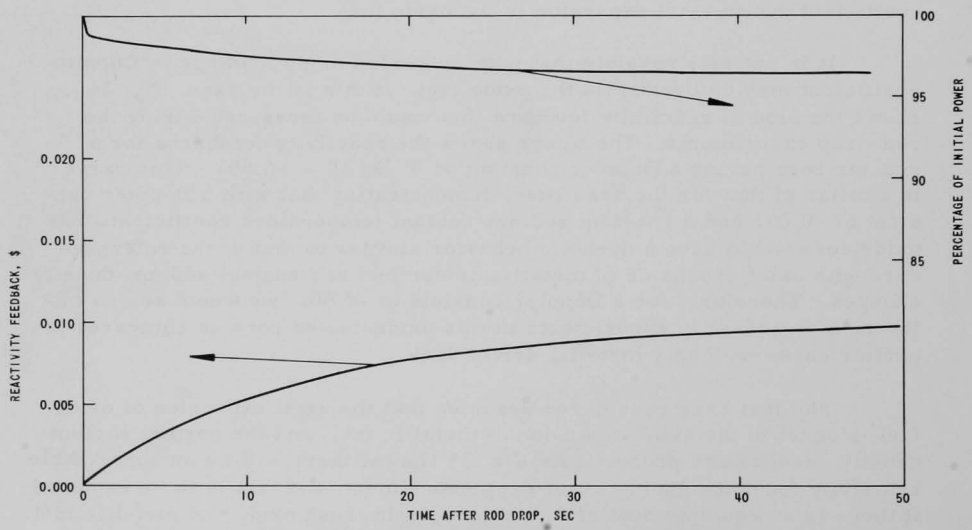

Fig. 33. Power and Reactivity Feedback following a Rod-drop Experiment at 50 MWt in a Predominantly Oxide-fuel Core, Assuming Feedback from Reduced Oxide-fuel Axial Expansion and Normal Sodium-density Changes. ANL Neg. No. ID-103-M5714.

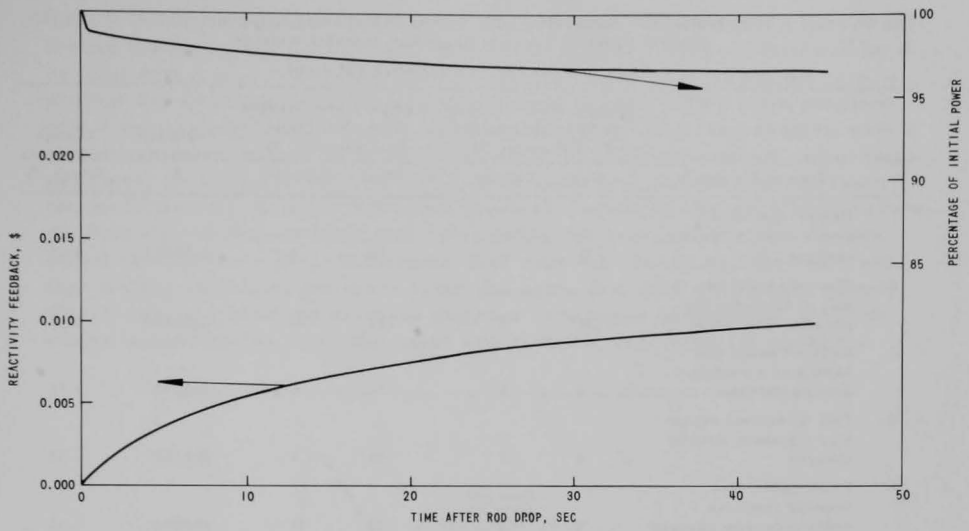

Fig. 34. Power and Reactivity Feedback following a Rod-drop Experiment at 50 MWt in a Predominantly Oxide-fuel Core, Assuming Oxide-fuel Doppler Constant = -0.001 and Sodium-density Changes. ANL Neg. No. ID-103-M5715.

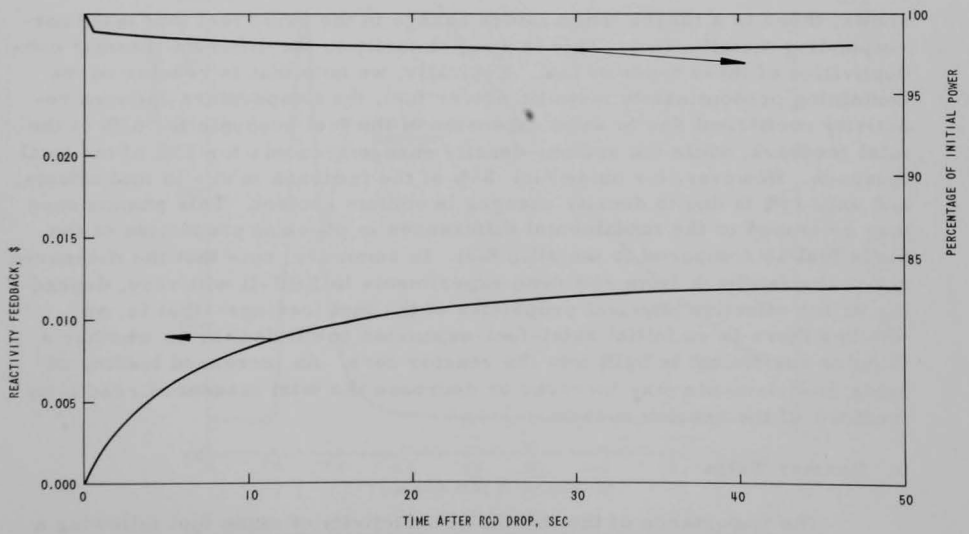

Fig. 35. Power and Reactivity Feedback following a Rod-drop Experiment at 50 MWt in a Predominantly Oxide-fuel Core, Assuming Feedback from Sodium-density Changes and Oxide-fuel Axial Expansion = Metal-fuel Axial Expansion. ANL Neg. No. ID-103-M5716.

TABLE IX. Comparison of Rod-drop Experiments Assuming Several Different Types of Reactivity-feedback Sources

(Data compared at 40.0 sec after rod drop)

Case No.	Type of Feedback	Temperature Changes in Typical Metallic Fuel Element, °F		Temperature Changes in Typical Oxide Fuel Element, °F		Feedback Reactivity, $	Change in Reactor Power, %
		Fuel	Sodium	Fuel	Sodium		
1	Driver-fuel expansion + sodium-density changes	11	3	86	7	0.00807	4.01
2	No oxide feedback; only sodium-density changes from oxide	16	5	121	10	0.00446	5.71
3	Reduced oxide-fuel expansion + sodium-density changes	9	3	74	6	0.00937	3.44
4	Full oxide-fuel expansion + sodium-density changes	6	2	51	4	0.01120	2.38
5	Small oxide-fuel Doppler feedback + sodium-density changes	9	3	72	6	0.00953	3.35
6	Oxide-fuel axial expansion = driver-fuel axial expansion + sodium-density changes	6	2	45	4	0.01171	2.05

shows, there is a larger temperature change in the oxide fuel than in the corresponding metallic fuel. This is due primarily to the different thermal conductivities of these types of fuel. Typically, we note that in reactor cores containing predominantly metallic driver fuel, the temperature-induced reactivity coefficient due to axial expansion of the fuel accounts for 67% of the total feedback, while the sodium-density change accounts for 33% of the total feedback. However, for oxide fuel, 85% of the feedback is due to fuel effects, and only 15% is due to density changes in sodium coolant. This phenomenon may be traced to the fundamental differences in physical properties of the oxide fuel as compared to metallic fuel. In summary, note that the measured reactivity feedback from rod-drop experiments in EBR-II will vary, depending on the effective physical properties of the fuel loadings--that is, on whether there is an initial axial-fuel-expansion coefficient or on whether a Doppler coefficient is built into the reactor core. An increased loading of oxide fuel elements may increase or decrease the total measured reactivity feedback of the reactor system.

B. Reactor Trips

The importance of the thermal conductivity of oxide fuel following a reactor trip has been mentioned above. The effect of this physical property of oxide fuel is to control the rate of heat removal from the fuel element, so that the oxide fuel remains at a higher temperature for a longer period of

time following a reactor trip. Figure 36 shows the temperature curves following the insertion of reactivity at a ramp rate of 1.0$/sec, followed by a reactor trip 1.5 sec after the start of the insertion. Following the trip, a prompt decay of the driver-fuel temperature occurs with a time constant of 0.3 sec, as opposed to a slow decay of the oxide-fuel temperature with a time constant of 4 sec. This is reflected in the sodium-coolant outlet temperature, as shown in Fig. 37. The temperature of sodium coolant from the metallic fuel exceeds that from the oxide, owing to the excellent thermal conductivity of the metallic fuel. Following the reactor trip, the coolant-outlet temperature from the driver-fuel element decays rapidly, whereas the coolant-outlet temperature from the oxide fuel element decays slowly. There can be a hundred or more degrees difference between the coolant-outlet temperatures from the oxide and metallic fuel-element channels.

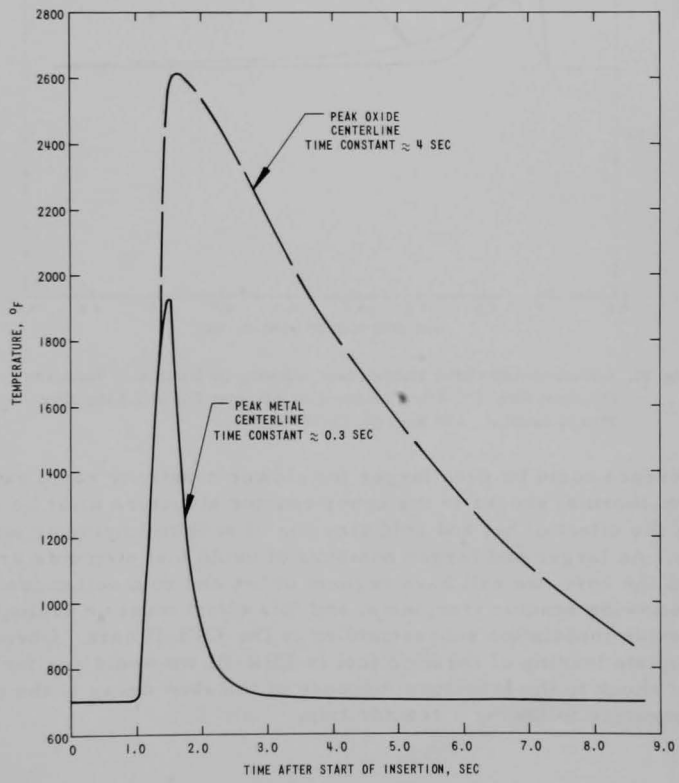

Fig. 36. Fuel Temperatures following the Insertion of Reactivity at a Ramp Rate of 1.0$/sec, Followed by a Reactor Trip at 1.5 sec after Start of Insertion. ANL Neg. No. ID-103-M5717.

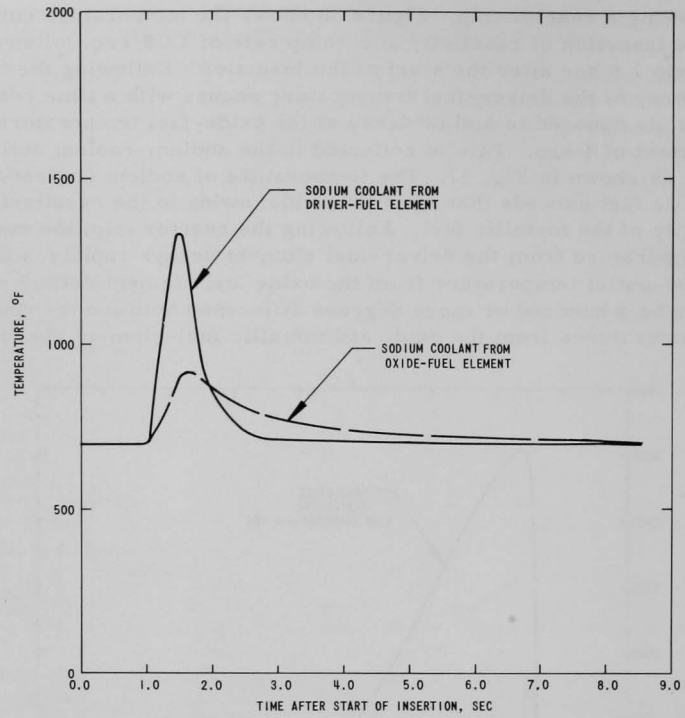

Fig. 37. Sodium-coolant Outlet Temperatures following the Insertion of Reactivity at a Ramp Rate of 1.0$/sec, Followed by a Reactor Trip at 1.5 sec after Start of Insertion. ANL Neg. No. ID-103-M5718.

This difference could be even larger for slower reactivity ramp rates. Therefore, thermal shocks to the upper reactor structure must be studied to assess the effect of hot and cold streams of sodium impinging on this structure. As larger and larger numbers of oxide fuel elements are introduced into the core, we will have regions of hot and cold outlet coolant during and following reactor transients, and this effect must be evaluated in locating oxide irradiation subassemblies in the EBR-II core. Obviously, for a complete loading of ceramic fuel in EBR-II, we would see far less of a thermal shock to the structure, because of the slow decay of the oxide-fuel temperature following a reactor trip.

VI. DYNAMIC BEHAVIOR DURING OPERATIONAL ABNORMALITIES

The primary intent of this report is to give operational guidance for future core loadings of predominantly oxide fuel. From this viewpoint, it is not useful to consider hypothetical component malfunctions such as fuel-handling accidents, since they do not, in themselves, give operational guidance. It is, however, considered credible, although of very low probability due to redundant plant-protective-system trip points, that an operational malfunction of a control rod or the safety rods may occur. Therefore, these operational malfunctions are considered to gain information related to the dynamic operating characteristics of an EBR-II core loaded predominantly with oxide fuel.

A. Full-power Operations

During normal full-power operations, an inadvertent movement of a control rod would be easily guarded against by the plant-protective system. However, in the following studies to set up a figure of merit, it is assumed that an uncontrolled insertion of reactivity is introduced into the reactor during full-power operation, and the time required to reach the first point of peak-oxide-fuel melting is evaluated. (The figure of merit is taken to be the number of seconds to melting of oxide fuel. A larger figure of merit is a more desirable condition, implying a longer time to fuel melting.) Reactivity ramp rates from 0.001 to 0.1$/sec are considered. This more than spans the range of reactivity ramp rates anticipated from present or future high-worth control rods. Figure 38 shows the time to centerline

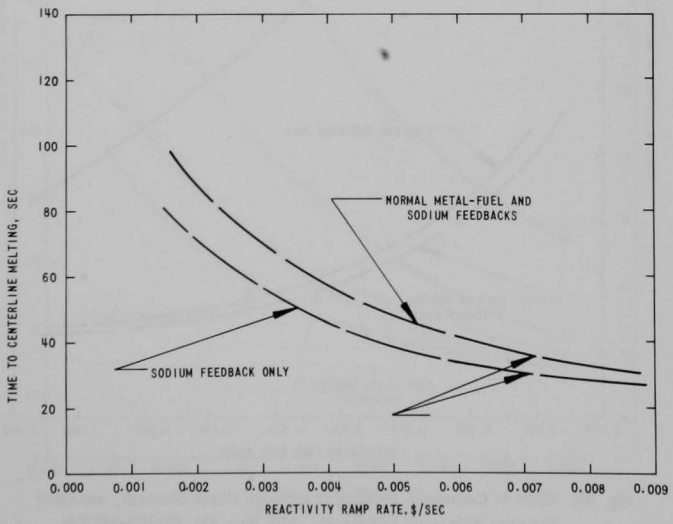

Fig. 38. Time to Centerline Melting in Average Oxide Element, Assuming Various Metal-core Feedbacks. ANL Neg. No. ID-103-M5719.

melting of oxide fuel for two assumed metal-core feedbacks, as a function of reactivity ramp rate. One curve shows the time to melting of oxide fuel, assuming the present normal prompt-feedback effects from metallic driver fuel and sodium. Cancelling out the fuel effect and leaving only the sodium-temperature reactivity effect is shown on the other curve. Even for reactivity ramps as high as 0.01$/sec, the time to centerline melting is greater than 20 sec, thus providing ample time for plant-protective-system action or for administrative control.

Figure 39 shows the time to centerline melting of oxide fuel for various reactivity ramp rates, assuming that the reactivity effect of oxide-fuel expansion is equal in magnitude to the reactivity effect of driver-fuel

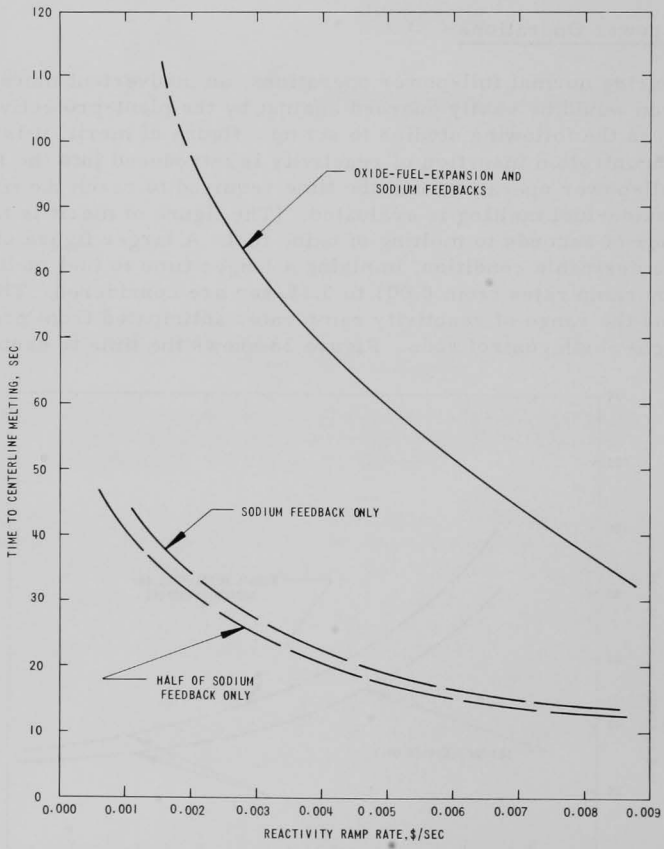

Fig. 39. Time to Centerline Melting in Average Oxide Element, Assuming Various Oxide-core Feedbacks. ANL Neg. No. ID-103-M5720.

expansion, and assuming normal sodium-coolant density effects. As indicated, the times to centerline melting are approximately equal to the times obtained with only reactivity effects from driver-fuel expansion. For no fuel expansion in the oxide and only sodium-density effects, the curves converge at ≈0.01$/sec to a time to melting of slightly over 10 sec--which is lower by a factor of 2 than the time for cores protected by driver-fuel feedback. However, this still provides ample time for plant-protective-system action or administrative control.

Finally, as noted in Section V.A above, a Doppler coefficient may be present in oxide fuel. To assess this effect, Doppler constants, $T\,\partial k/\partial T$, from 0.00 to -0.004 were considered. Figure 40 presents the results of

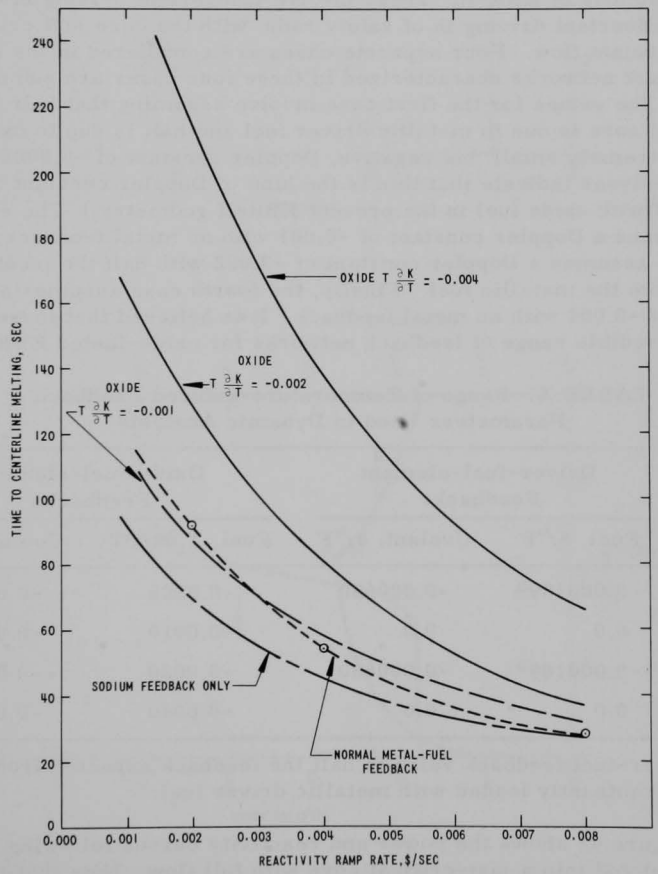

Fig. 40. Time to Centerline Melting in Average Oxide Element, Assuming Various Feedbacks from Oxide Doppler and from Metal Fuel (sodium feedback included in all cases). ANL Neg. No. ID-103-M5721.

these studies, indicating that for increasingly negative Doppler constants, the time to melting is appreciably lengthened. The figure shows that for a Doppler constant of -0.001, the time to melting is very similar to that for oxide elements protected by normal metallic-driver-fuel feedback. These conclusions are similar to the conclusions drawn in the rod-drop studies, which indicate that the feedback networks in a predominantly oxide core with a Doppler constant of -0.001 would be nearly identical to those for the present metallic-driver-fuel core in EBR-II.

B. Startup

Two low-probability malfunctions of components are considered for the startup mode of EBR-II. These involve inadvertent driving in of a control rod, or inadvertent driving in of safety rods, with the core just critical and with full coolant flow. Four separate cases are considered in the analysis. The feedback networks characterized in these four cases are summarized in Table X. The values for the first case involve assuming that half the feedback in the core is due to metallic driver fuel and half is due to oxide fuel with an extremely small, but negative, Doppler constant of -0.0005. (Recent nuclear analyses indicate that this is the kind of Doppler constant that would be present with oxide fuel in the present EBR-II geometry.) The second case assumes a Doppler constant of -0.001 with no metal feedback. The third case assumes a Doppler constant of -0.002 with half the feedback coming from the metallic fuel. Finally, the fourth case assumes a Doppler constant of -0.004 with no metal feedback. It is believed that these cases span the credible range of feedback networks for oxide-fueled EBR-II cores.

TABLE X. Range of Temperature-induced Feedback Parameters Used in Dynamic Analysis

Case Number	Driver-fuel-element Feedbacks		Oxide-fuel-element Feedbacks	
	Fuel, $/°F	Coolant, $/°F	Fuel, T ∂k/∂T	Coolant, $/°F
1	-0.000189[a]	-0.000680	-0.0005	-0.000621
2	0.0	0.0	-0.0010	-0.000621
3	-0.000189[a]	-0.000680	-0.0020	-0.000621
4	0.0	0.0	-0.0040	-0.000621

[a]This driver-fuel feedback value is half the feedback expected from a core predominantly loaded with metallic driver fuel.

Figure 41 shows the power and reactivity curves following the driving of a control rod into a just-critical core with full flow. Note that the reactivity feedback turns the power burst downward. In Fig. 42 the peak driver-fuel temperatures are presented following this inadvertent driving of a

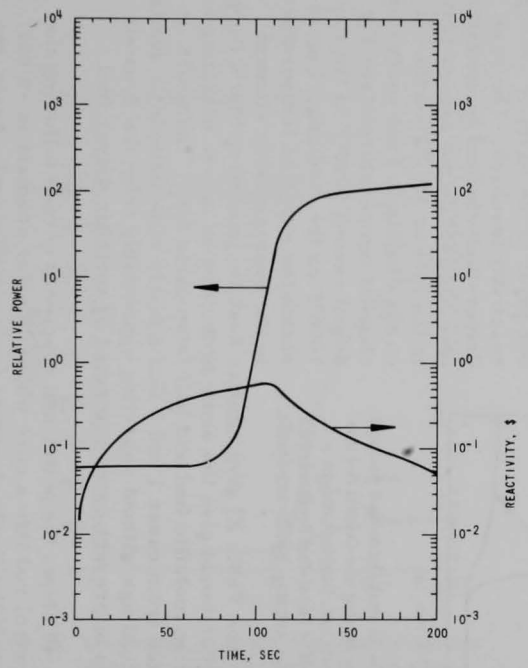

Fig. 41. Power and Reactivity Curves following the Driving of a Control Rod into a Just-critical Core; Doppler Constant = -0.0005; Half of Metal-fuel Feedback; Full Coolant Flow. ANL Neg. No. ID-103-M5722.

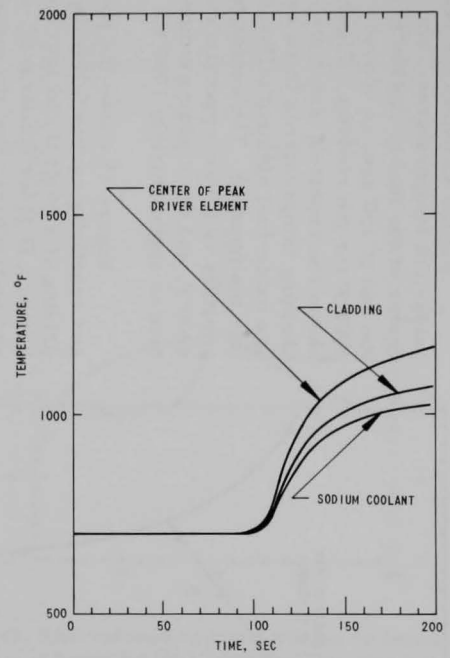

Fig. 42. Temperatures in Peak Driver-fuel Element following the Driving of a Control Rod into a Just-critical Core; Doppler Constant = -0.0005; Half of Metal-fuel Feedback; Full Coolant Flow. ANL Neg. No. ID-103-M5723.

control rod into a just-critical core. The peak driver-fuel temperature, 150 sec after the start of the insertion, reaches a level of 1100°F, whereas the cladding is approximately 1000°F.

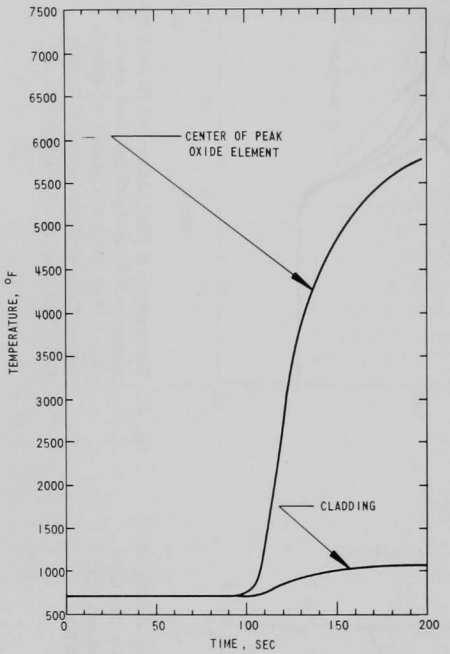

Fig. 43. Temperatures in Peak Oxide-fuel Element following the Driving of a Control Rod into a Just-critical Core; Doppler Constant = -0.0005; Half of Metal-fuel Feedback; Full Coolant Flow. ANL Neg. No. ID-103-M5724.

Figure 43 shows the peak oxide-fuel temperatures. The center of the fuel is at 4900°F at the end of 150 sec, as opposed to 1000°F for the cladding. Figure 44 shows the expected center and cladding temperatures in an average oxide-fuel element following this malfunction. The center temperature is lower, approximately 4200°F, and the cladding temperature is approximately 1000°F.

Figure 45 shows the power and reactivity curves following the driving of a control rod into a core having a Doppler constant of -0.001 and no feedback from the metallic fuel. As the figure indicates, the reactivity is limited to approximately 60¢ prior to the onset of the negative reactivity feedback. The peak driver-fuel-element temperatures (see Fig. 46) do not exceed 1110°F in the fuel or 1010°F on the hot spot on the cladding. Peak oxide-fuel-element temperatures (see Fig. 47) do not exceed 5000°F in the fuel or 1000°F on the cladding. Figure 48 shows the expected temperatures in the average oxide element. Cases 1 and 2 (see Table X) give similar results, indicating that a Doppler constant of -0.001 would give the same protection as a core obtaining half its feedback from metallic fuel and half from oxide fuel. Therefore, it can be concluded from cases 1 and 2 that a fairly wide latitude is available in oxide core loadings without departing appreciably from the dynamic characteristics of present cores protected by metallic driver fuel.

Figure 49 shows the power and reactivity curves following the driving of a control rod into a core whose Doppler constant is -0.002, assuming that half the feedback comes from metallic fuel. Again, the reactivity is limited to approximately 60¢, and the prompt feedbacks turn the power burst around. Figure 50 shows the peak driver-fuel temperatures,

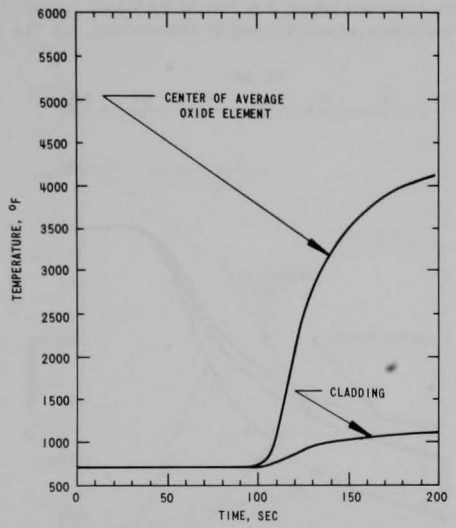

Fig. 44. Temperatures in Average Oxide-fuel Element following the Driving of a Control Rod into a Just-critical Core; Doppler Constant = -0.0005; Half of Metal-fuel Feedback; Full Coolant Flow. ANL Neg. No. ID-103-M5725.

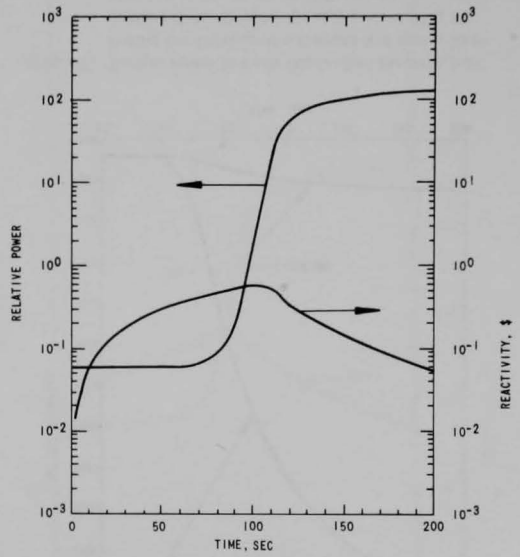

Fig. 45. Power and Reactivity Curves following the Driving of a Control Rod into a Just-critical Core; Doppler Constant = -0.001; No Metal-fuel Feedback; Full Coolant Flow. ANL Neg. No. ID-103-M5726.

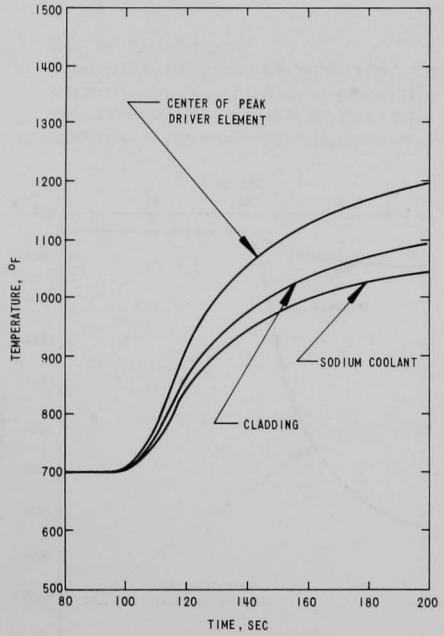

Fig. 46. Temperatures in Peak Driver-fuel Element following the Driving of a Control Rod into a Just-critical Core; Doppler Constant = -0.001; No Metal-fuel Feedback; Full Coolant Flow. ANL Neg. No. ID-103-M5727.

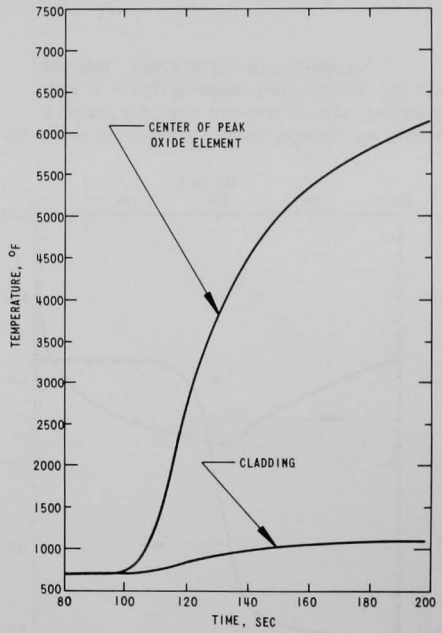

Fig. 47. Temperatures in Peak Oxide-fuel Element following the Driving of a Control Rod into a Just-critical Core; Doppler Constant = -0.001; No Metal-fuel Feedback; Full Coolant Flow. ANL Neg. No. ID-103-M5728.

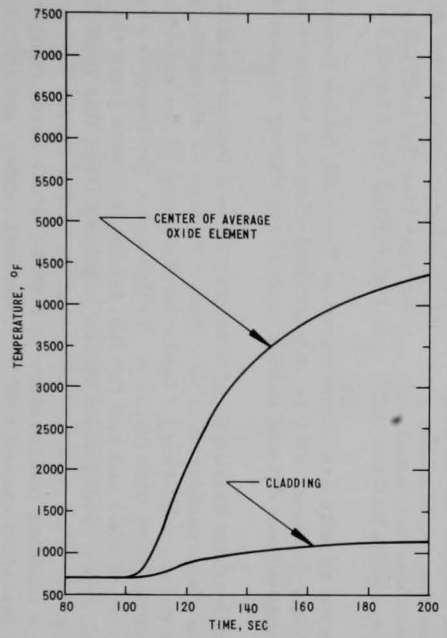

Fig. 48. Temperatures in Average Oxide-fuel Element following the Driving of a Control Rod into a Just-critical Core; Doppler Constant = -0.001; No Metal-fuel Feedback; Full Coolant Flow. ANL Neg. No. ID-103-M5729.

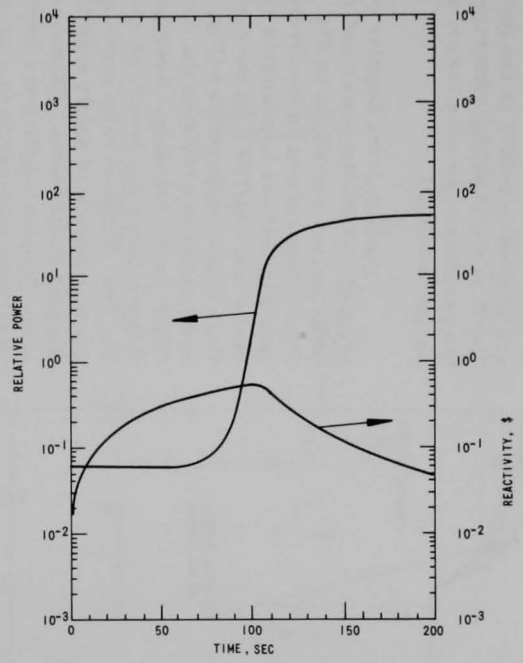

Fig. 49. Power and Reactivity Curves following the Driving of a Control Rod into a Just-critical Core; Doppler Constant = -0.002; Half of Metal-fuel Feedback; Full Coolant Flow. ANL Neg. No. ID-103-M5730.

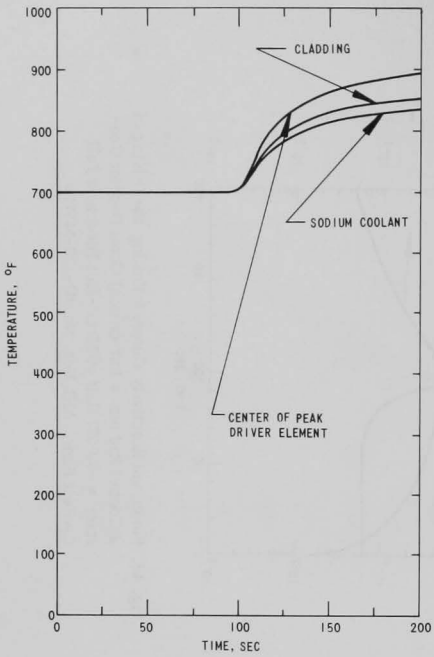

Fig. 50. Temperatures in Peak Driver-fuel Element following the Driving of a Control Rod into a Just-critical Core; Doppler Constant = -0.002; Half of Metal-fuel Feedback; Full Coolant Flow. ANL Neg. No. ID-103-M5731.

which are now limited to 850°F in the fuel and 820°F on the cladding. Peak oxide-fuel temperatures for a Doppler constant of -0.002 (Fig. 51) are limited to 2500°F in the fuel and 850°F on the cladding. Average oxide temperatures are even lower, as shown in Fig. 52.

Finally, for a Doppler constant of -0.004, the power and reactivity curves are shown in Fig. 53. Peak temperatures in the driver fuel (see Fig. 54) are now limited to 800°F in the fuel and 770°F on the cladding. Peak oxide temperatures (Fig. 55) are limited to 1750°F in the fuel and 780°F on the cladding. Average oxide temperatures are lower, as shown in Fig. 56. These results imply a greater degree of safety with large Doppler coefficients. (However, large Doppler coefficients imply beryllium moderation to a greater degree, leading to appreciable moderation of the fast-neutron irradiation spectrum, and this is considered undesirable in view of the research programs that the LMFBR program has identified for EBR-II.)

The above results are summarized in Table XI, which compares the various reactivity-feedback effects on peak-fuel-element temperatures following the inadvertent driving in of a control rod during reactor startup.

The inadvertent driving in of a safety rod is a low-probability malfunction that is also considered in this study. Figure 57 shows the power and reactivity curves following an inadvertent driving of the safety rods into a just-critical core with full flow. In this case, the Doppler constant is assumed to be -0.0005 and half the fuel feedback comes from the metallic fuel. The peak driver-fuel temperatures resulting from this insertion are depicted in Fig. 58. The peak fuel temperature in the driver fuel is 1200°F, as opposed to a cladding temperature of 1100°F. Peak oxide temperatures following this insertion exceed 6300°F at the fuel center, and the cladding is 1000°F at the hot spot (see Fig. 59). The average oxide temperatures are lower (see Fig. 60). At the end of 150 sec, the average oxide fuel would be approaching centerline melting and the cladding temperature would be approaching 1100°F.

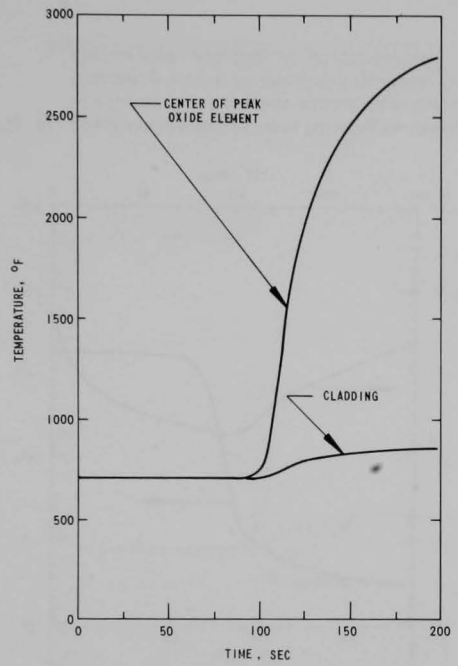

Fig. 51. Temperatures in Peak Oxide-fuel Element following the Driving of a Control Rod into a Just-critical Core; Doppler Constant = -0.002; Half of Metal-fuel Feedback; Full Coolant Flow. ANL Neg. No. ID-103-M5732.

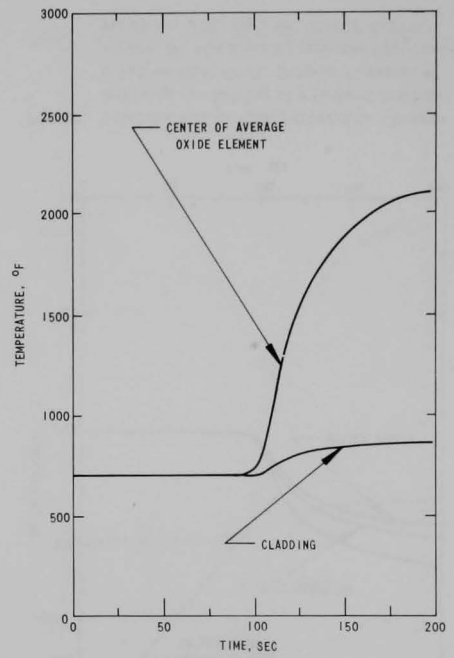

Fig. 52. Temperatures in Average Oxide-fuel Element following the Driving of a Control Rod into a Just-critical Core; Doppler Constant = -0.002; Half of Metal-fuel Feedback; Full Coolant Flow. ANL Neg. No. ID-103-M5733.

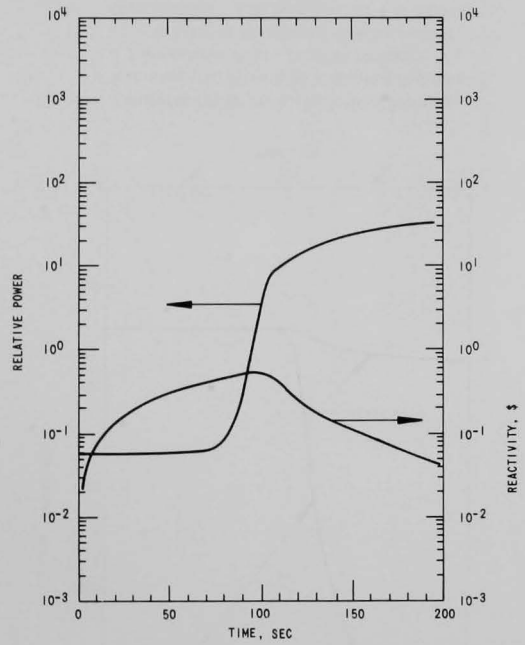

Fig. 53. Power and Reactivity Curves following the Driving of a Control Rod into a Just-critical Core; Doppler Constant = -0.004; No Metal-fuel Feedback; Full Coolant Flow. ANL Neg. No. ID-103-M5734.

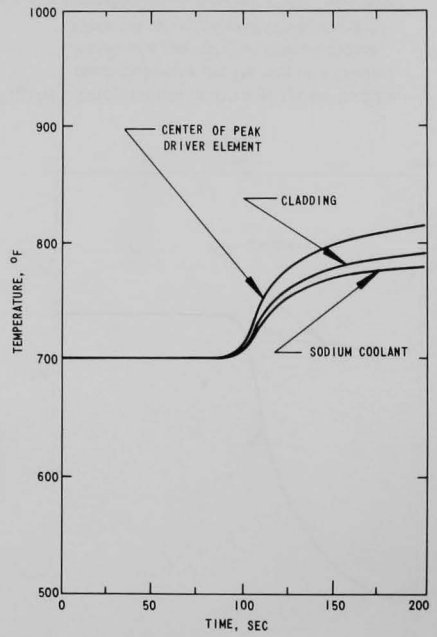

Fig. 54. Temperatures in Peak Driver-fuel Element following the Driving of a Control Rod into a Just-critical Core; Doppler Constant = -0.004; No Metal-fuel Feedback; Full Coolant Flow. ANL Neg. No. ID-103-M5735.

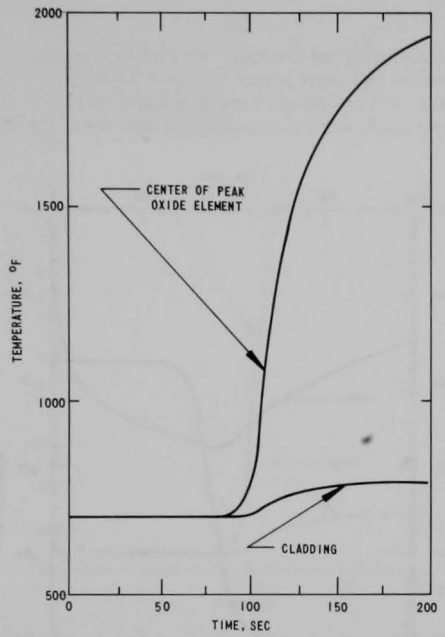

Fig. 55. Temperatures in Peak Oxide-fuel Element following the Driving of a Control Rod into a Just-critical Core; Doppler Constant = -0.004; No Metal-fuel Feedback; Full Coolant Flow. ANL Neg. No. ID-103-M5736.

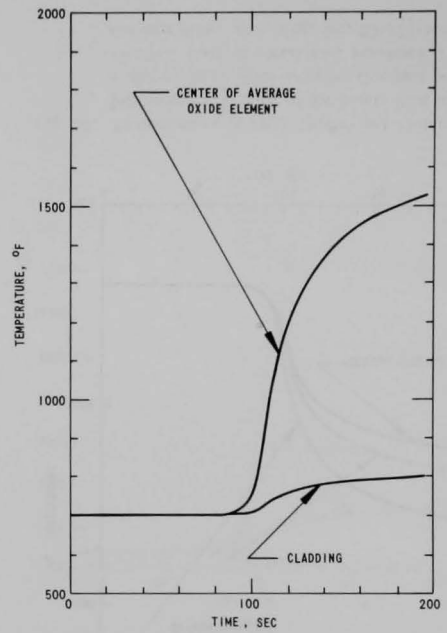

Fig. 56. Temperatures in Average Oxide-fuel Element following the Driving of a Control Rod into a Just-critical Core; Doppler Constant = -0.004; No Metal-fuel Feedback; Full Coolant Flow. ANL Neg. No. ID-103-M5737.

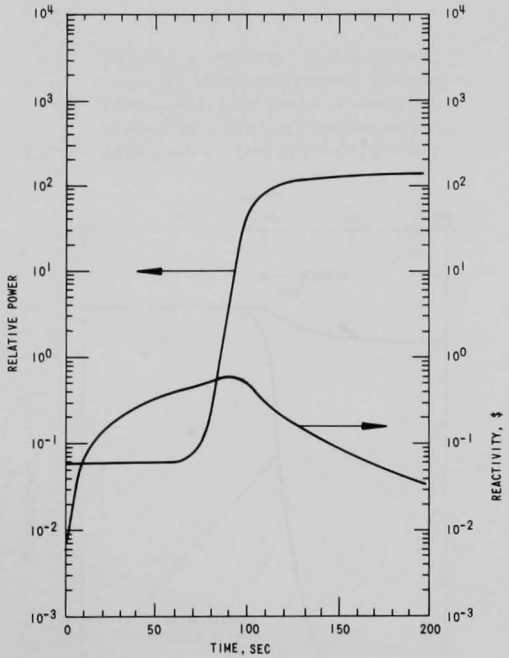

Fig. 57. Power and Reactivity Curves following the Driving of the Safety Rods into a Just-critical Core; Doppler Constant = -0.0005; Half of Metal-fuel Feedback; Full Coolant Flow. ANL Neg. No. ID-103-M5738.

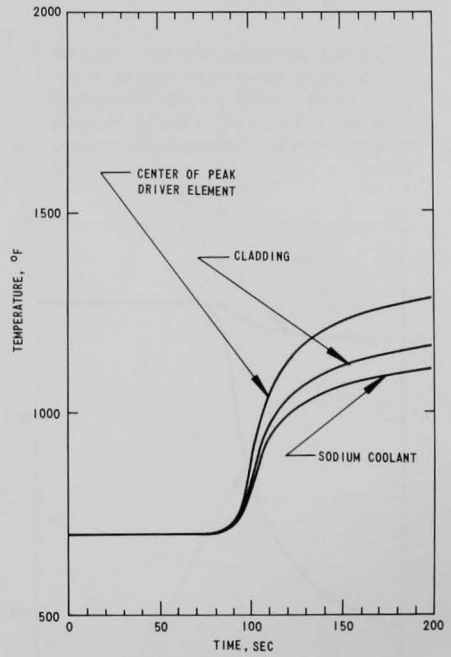

Fig. 58. Temperatures in Peak Driver-fuel Element following the Driving of the Safety Rods into a Just-critical Core; Doppler Constant = -0.0005; Half of Metal-fuel Feedback; Full Coolant Flow. ANL Neg. No. ID-103-M5739.

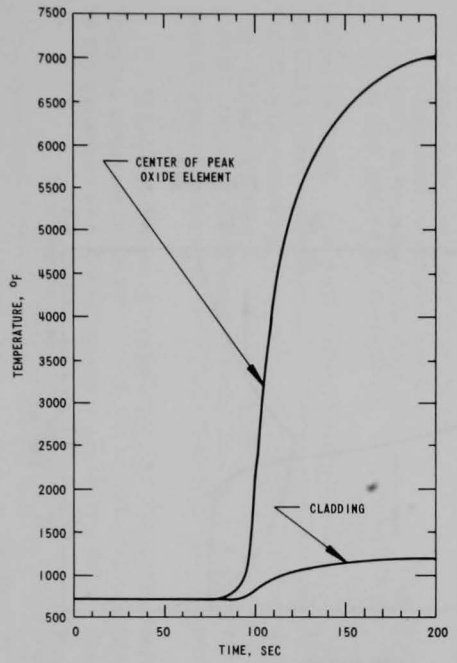

Fig. 59. Temperatures in Peak Oxide-fuel Element following the Driving of the Safety Rods into a Just-critical Core; Doppler Constant = -0.0005; Half of Metal-fuel Feedback; Full Coolant Flow. ANL Neg. No. ID-103-M5740.

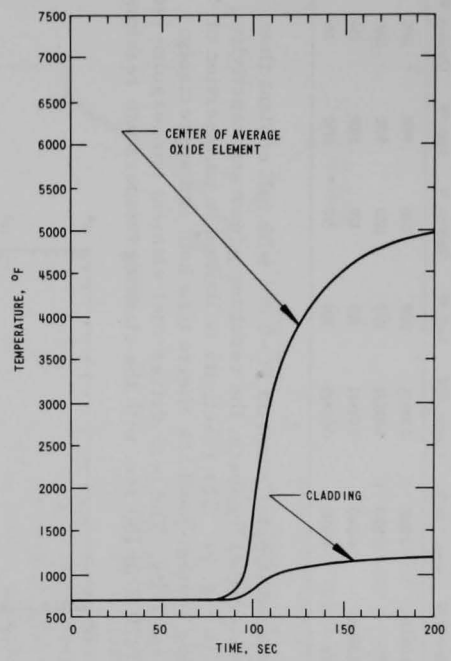

Fig. 60. Temperatures in Average Oxide-fuel Element following the Driving of the Safety Rods into a Just-critical Core; Doppler Constant = -0.0005; Half of Metal-fuel Feedback; Full Coolant Flow. ANL Neg. No. ID-103-M5741.

TABLE XI. Comparison of Various Reactivity-feedback Effects on Peak Fuel-element Temperatures following an Inadvertent Driving In of a Control Rod during Reactor Startup

	Feedback from Driver-fuel Element		Feedback from Oxide-fuel Element		Temperatures in Peak Driver-fuel Element 150 sec after Start of Insertion		Temperatures in Peak Oxide-fuel Element 150 sec after Start of Insertion	
Case No.	Fuel, $/°F	Coolant, $/°F	Fuel, T ∂k/∂T	Coolant, $/°F	Fuel, °F	Cladding, °F	Fuel, °F	Cladding, °F
1	-0.000189	-0.000680	-0.0005	-0.000621	1100	1000	4900	1000
2	0.0	0.0	-0.0010	-0.000621	1110	1010	5000	1000
3	-0.000189	-0.000680	-0.0020	-0.000621	850	820	2500	850
4	0.0	0.0	-0.0040	-0.000621	800	770	1750	780

For an assumed Doppler constant of -0.001 with full coolant flow and no metallic-driver-fuel feedback, the resulting power and reactivity curves are shown in Fig. 61. The reactivity is limited to an insertion of less than 70¢ before system-feedback effects take hold and appreciably reduce the total reactivity. The peak driver-fuel-element temperature (see Fig. 62) reaches 1270°F in 150 sec, with the cladding temperature reaching

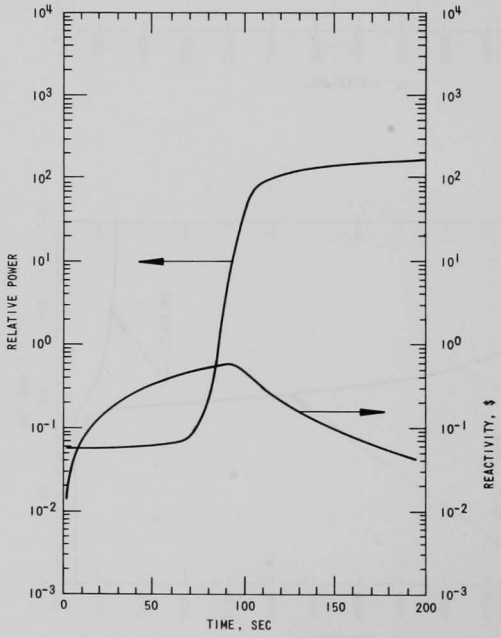

Fig. 61. Power and Reactivity Curves following the Driving of the Safety Rods into a Just-critical Core; Doppler Constant = -0.001; No Metal-fuel Feedback; Full Coolant Flow. ANL Neg. No. ID-103-M5742.

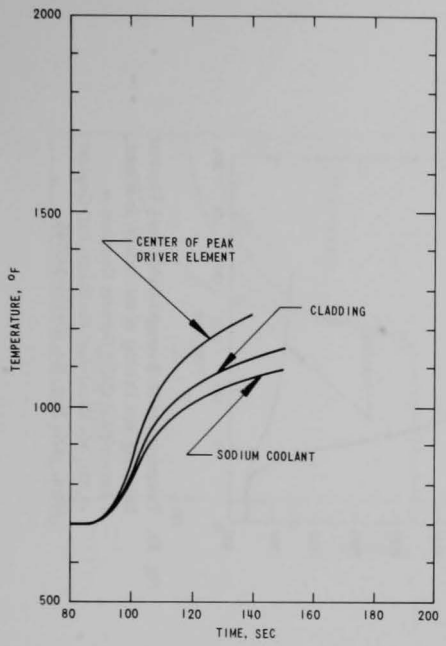

Fig. 62. Temperatures in Peak Driver-fuel Element following the Driving of the Safety Rods into a Just-critical Core; Doppler Constant = -0.001; No Metal-fuel Feedback; Full Coolant Flow. ANL Neg. No. ID-103-M5743.

1110°F. Peak oxide temperatures (see Fig. 63) are higher than in the previous case, approaching 7000°F in the fuel and 1020°F in the cladding. The average oxide temperatures (see Fig. 64) approach centerline melting, with a cladding temperature approaching 1100°F.

Figure 65 shows power and reactivity for the case in which half the driver-fuel feedback is present and there is a Doppler constant of -0.002. Peak driver-fuel temperatures are now limited appreciably by the Doppler feedback to a value of 910°F in the peak driver fuel and 870°F on the cladding (Fig. 66). Peak oxide temperatures are also appreciably limited to 3000°F in the hottest spot in the oxide-fuel element, with the cladding temperature approaching 900°F (Fig. 67). Average oxide temperatures (Fig. 68) approach 2500°F in the fuel and 900°F on the cladding.

Figure 69 shows power and reactivity for the case in which the Doppler constant is -0.004 with no metal feedback. The peak driver-fuel-element temperatures are greatly limited by this large Doppler constant, approaching 820°F in the fuel and 790°F in the cladding (as shown in Fig. 70). Peak oxide temperatures (see Fig. 71) are limited to ≈2050°F, with the cladding temperature limited to 850°F. Average oxide temperatures (shown in Fig. 72) are appreciably lower, approaching approximately 1650°F in the fuel center.

These results are summarized in Table XII, which indicates that a Doppler constant of -0.0005 to -0.001 would yield similar characteristics to the present core of predominantly metallic driver fuel.

TABLE XII. Comparison of Various Reactivity-feedback Effects on Peak Fuel-element Temperatures following an Inadvertent Driving In of the Safety Rods during Reactor Startup

	Feedback from Driver-fuel Element		Feedback from Oxide-fuel Element		Temperatures in Peak Driver-fuel Element 150 sec after Start of Insertion		Temperatures in Peak Oxide-fuel Element 150 sec after Start of Insertion	
Case No.	Fuel, $/°F	Coolant, $/°F	Fuel, T ∂k/∂T	Coolant, $/°F	Fuel, °F	Cladding, °F	Fuel, °F	Cladding, °F
1	-0.000189	-0.000680	-0.0005	-0.000621	1200	1100	6300	1000
2	0.0	0.0	-0.0010	-0.000621	1270	1110	7000	1040
3	-0.000189	-0.000680	-0.0020	-0.000621	910	870	3000	900
4	0.0	0.0	-0.0040	-0.000621	820	790	2050	850

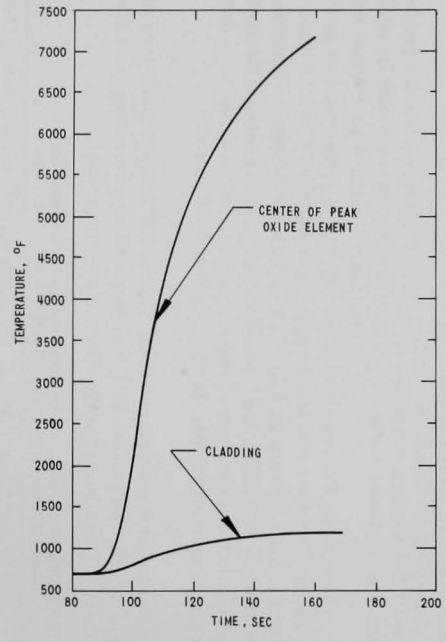

Fig. 63. Temperatures in Peak Oxide-fuel Element following the Driving of the Safety Rods into a Just-critical Core; Doppler Constant = -0.001; No Metal-fuel Feedback; Full Coolant Flow. ANL Neg. No. ID-103-M5744.

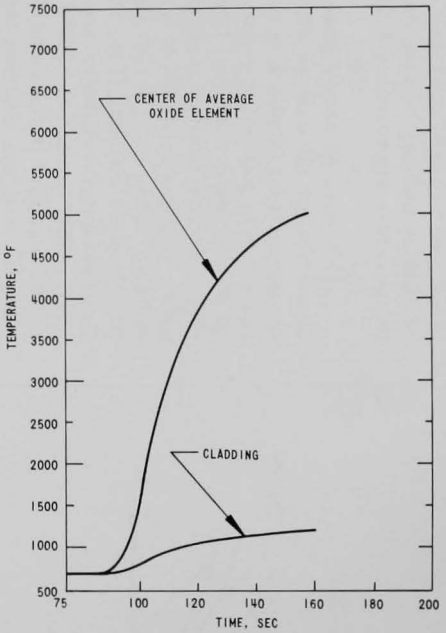

Fig. 64. Temperatures in Average Oxide-fuel Element following the Driving of the Safety Rods into a Just-critical Core; Doppler Constant = -0.001; No Metal-fuel Feedback; Full Coolant Flow. ANL Neg. No. ID-103-M5745.

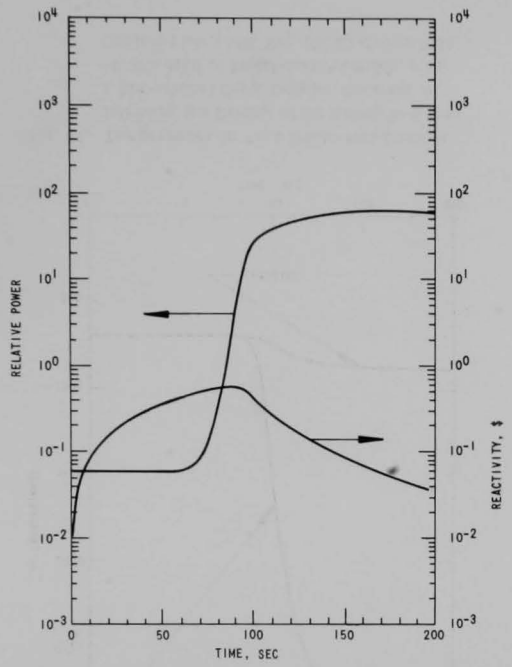

Fig. 65. Power and Reactivity Curves following the Driving of the Safety Rods into a Just-critical Core; Doppler Constant = -0.002; Half of Metal-fuel Feedback; Full Coolant Flow. ANL Neg. No. ID-103-M5746.

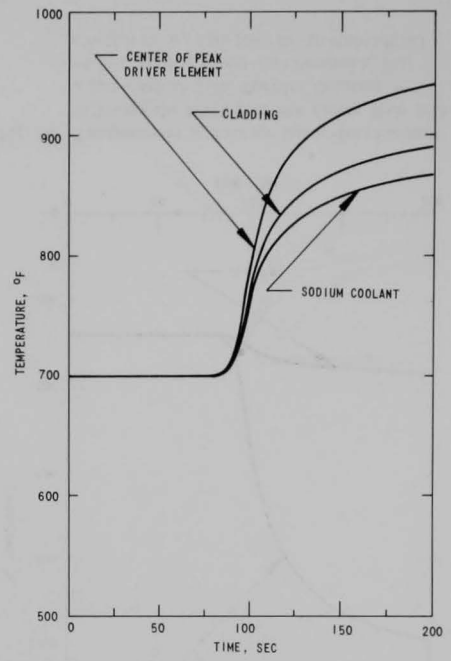

Fig. 66. Temperatures in Peak Driver-fuel Element following the Driving of the Safety Rods into a Just-critical Core; Doppler Constant = -0.002; Half of Metal-fuel Feedback; Full Coolant Flow. ANL Neg. No. ID-103-M5747.

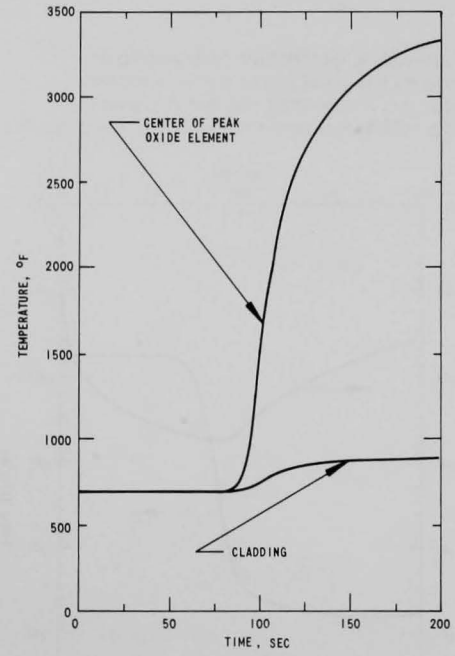

Fig. 67. Temperatures in Peak Oxide-fuel Element following the Driving of the Safety Rods into a Just-critical Core; Doppler Constant = -0.002; Half of Metal-fuel Feedback; Full Coolant Flow. ANL Neg. No. ID-103-M5748.

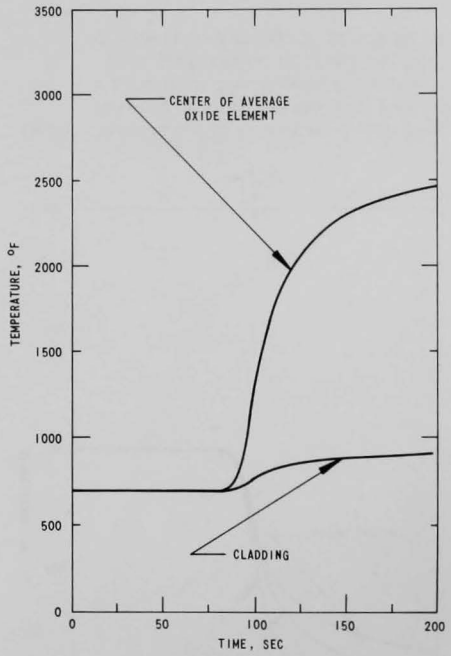

Fig. 68. Temperatures in Average Oxide-fuel Element following the Driving of the Safety Rods into a Just-critical Core; Doppler Constant = -0.002; Half of Metal-fuel Feedback; Full Coolant Flow. ANL Neg. No. ID-103-M5749.

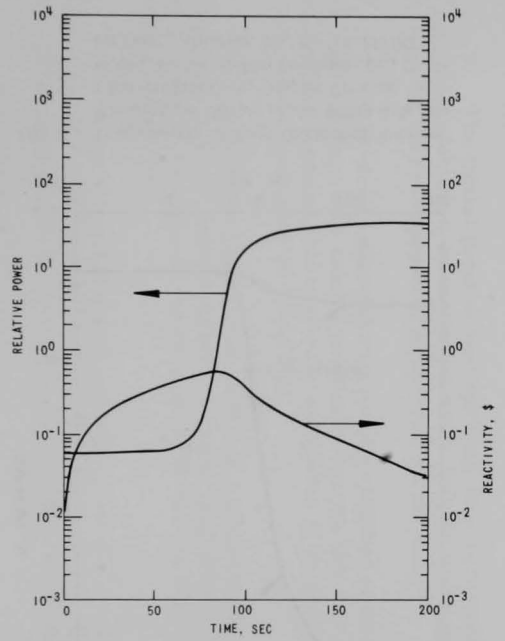

Fig. 69. Power and Reactivity Curves following the Driving of the Safety Rods into a Just-critical Core; Doppler Constant = -0.004; No Metal-fuel Feedback; Full Coolant Flow. ANL Neg. No. ID-103-M5750.

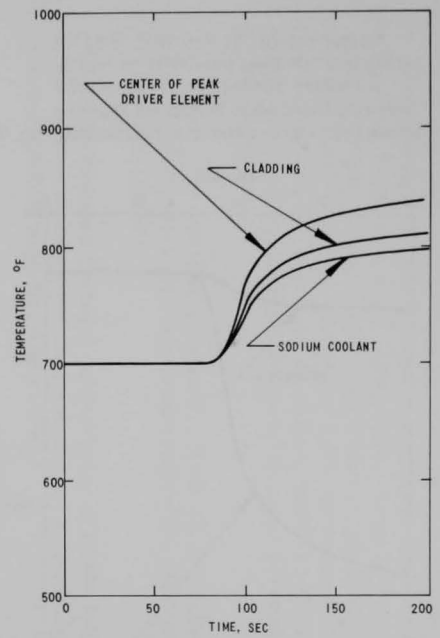

Fig. 70. Temperatures in Peak Driver-fuel Element following the Driving of the Safety Rods into a Just-critical Core; Doppler Constant = -0.004; No Metal-fuel Feedback; Full Coolant Flow. ANL Neg. No. ID-103-M5751.

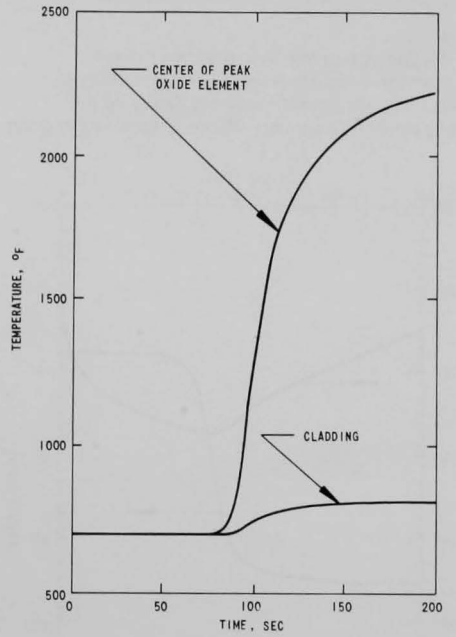

Fig. 71. Temperatures in Peak Oxide-fuel Element following the Driving of the Safety Rods into a Just-critical Core; Doppler Constant = -0.004; No Metal-fuel Feedback; Full Coolant Flow. ANL Neg. No. ID-103-M5752.

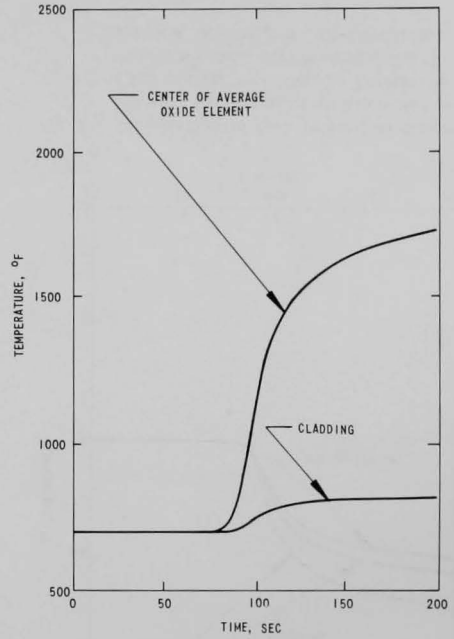

Fig. 72. Temperatures in Average Oxide-fuel Element following the Driving of the Safety Rods into a Just-critical Core; Doppler Constant = -0.004; No Metal-fuel Feedback; Full Coolant Flow. ANL Neg. No. ID-103-M5753.

VII. SUMMARY AND CONCLUSIONS

The influence of predominantly oxide fuel loadings on the operational characteristics of EBR-II has been investigated by means of a dynamic simulation of the neutronic, thermal, and hydraulic characteristics of a reactor core having feedback networks typical of oxide fuel. Routine reactor operations have been studied by simulating rod-drop experiments and automatic reactor trips. Operational abnormalities caused by hypothetical malfunctions of a control rod or the safety rods have been analyzed for meaningful departures from the behavior shown in past studies with metallic fuel. The main conclusions obtained from the investigations presented in this report are briefly listed below:

1. Over the operating range for EBR-II, an increased loading of oxide-fuel subassemblies will not compromise the inherent safety of EBR-II as an irradiation facility.

2. The reduced thermal conductivity of oxide fuel is the main cause of the different transient characteristics of oxide fuel as compared to the present EBR-II metallic driver fuel.

3. The reduced thermal conductivity of oxide fuel elements will cause a mismatch in the decay of sodium outlet temperatures following an automatic reactor trip.

4. The initial point of fuel melting, in a core containing oxide and metallic fuel elements, is dependent on reactivity ramp rate, coolant flow rate, and the inherent physical properties of the fuel.

5. Rod-drop experimental results obtained from predominantly oxide fuel loadings will exhibit similar response times to predominantly metallic fuel loadings, but may vary somewhat in magnitude depending on the irradiation behavior of oxide fuel.

6. A Doppler constant of -0.001 in a predominantly oxide fuel loading plus normal sodium-density changes will produce an overall dynamic behavior similar to that of the present EBR-II core loading of predominantly metallic driver fuel.

7. An increased Doppler constant of -0.002 to -0.004 will provide greater inherent transient protection in oxide-fueled cores, but the associated softer neutron spectrum may be undesirable for irradiation tests.

APPENDIX A

Fuel-handling Malfunctions

Malfunctions of components during fuel handling, leading to changes in reactor parameters, are highly hypothetical occurrences and therefore afford no operational guidance. However, since reference is made in the Hazard Summary Report to these types of hypothetical occurrences, a few selected, assumed malfunctions are presented in this appendix.

The many failures in the fuel-handling circuitry and in administrative control required to set the initial conditions for these hypothetical occurrences are listed in Ref. 5. The malfunctions considered include high- and low-speed insertions of a central driver-fuel subassembly into a just-critical core under condition of convective flow of the primary coolant. The dropping of a central driver-fuel subassembly is also analyzed under these conditions. Two Doppler constants are considered, -0.0005 and -0.002, with one-half of the normal feedback from the metallic driver fuel.

1. Insertion of Central Subassembly at High Speed

(Doppler constant = -0.0005; half of metallic-fuel feedback)

The power and reactivity curves following the high-speed insertion of a central driver-fuel subassembly are presented in Fig. 73. The system reactivity reaches a peak of 0.96$ before the prompt negative feedbacks reduce the reactivity. The temperatures in the peak driver-fuel element, as shown in Fig. 74, reach 1800°F in the center of the fuel and 1750°F on the cladding 10 sec after the start of the insertion. Correspondingly, the peak oxide temperatures, as shown in Fig. 75, reach 2250°F in the center of the fuel and 1490°F on the cladding. The average oxide-fuel temperatures (Fig. 76) reach 2200°F in the fuel and only 1200°F on the cladding. The metallic-driver-fuel temperatures are high because only convective coolant is present, whereas the oxide-fuel temperatues are low because of the prompt temperature-induced reactivity feedback from sodium-density changes associated with the metallic driver-fuel elements.

2. Insertion of Central Subassembly at Low Speed

(Doppler constant = -0.002; half of metallic-fuel feedback)

The prompt response of the power and the system reactivity to the low-speed insertion of a central driver subassembly is presented in Fig. 77. The reactivity is limited to a peak of 0.70$ by the oxide Doppler constant and the metallic-driver-fuel feedbacks. The temperatures in the peak driver-fuel element (see Fig. 78) reach 1280°F in the fuel and 1200°F on

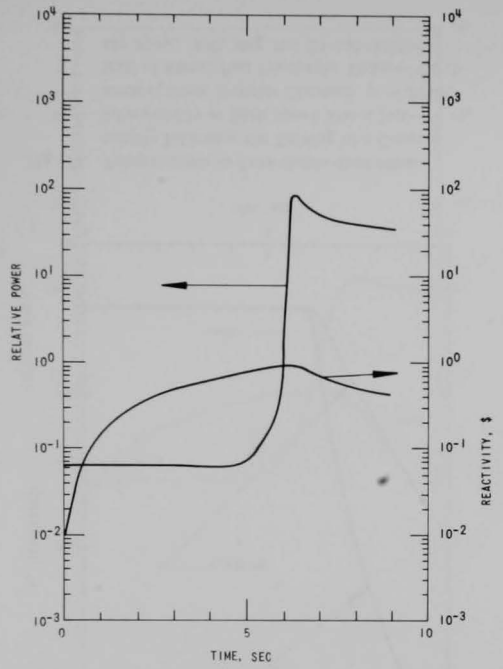

Fig. 73. Power and Reactivity Curves following the Driving of a Central Subassembly at High Speed into a Just-critical Core; Doppler Constant = -0.0005; Half of Metal-fuel Feedback; Reduced Coolant Flow. ANL Neg. No. ID-103-M5754.

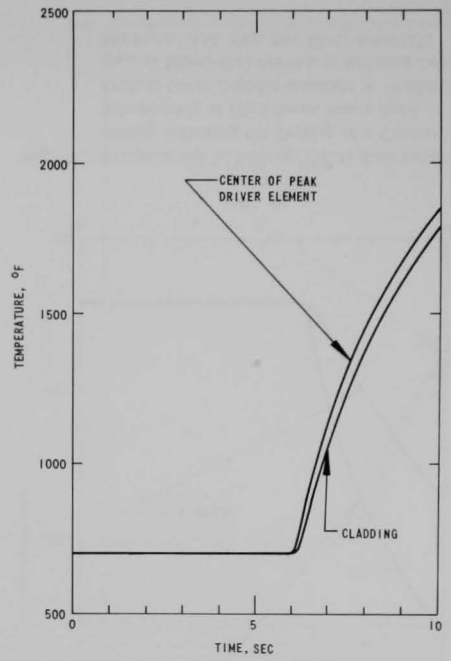

Fig. 74. Temperatures in Peak Driver-fuel Element following the Driving of a Central Subassembly at High Speed into a Just-critical Core; Doppler Constant = -0.0005; Half of Metal-fuel Feedback; Reduced Coolant Flow. ANL Neg No. ID-103-M5755.

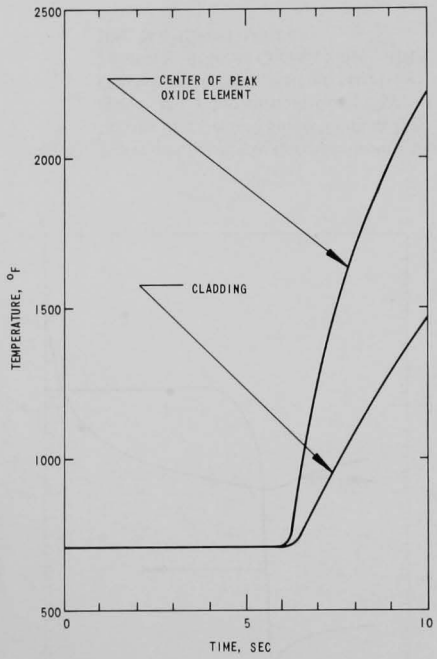

Fig. 75. Temperatures in Peak Oxide-fuel Subassembly following the Driving of a Central Subassembly at High Speed into a Just-critical Core; Doppler Constant = -0.0005; Half of Metal-fuel Feedback; Reduced Coolant Flow. ANL Neg. No. ID-103-M5756.

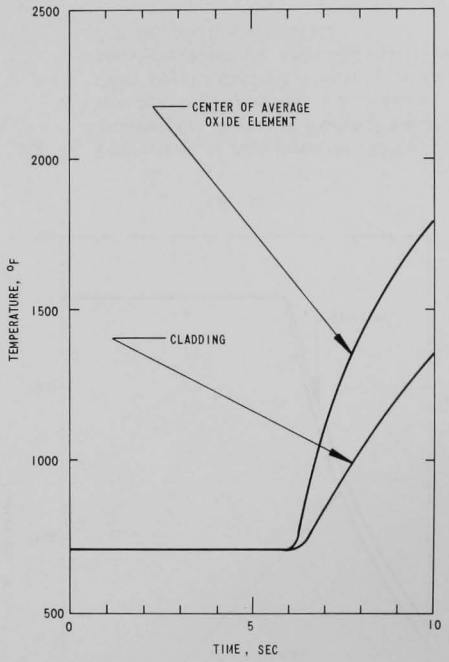

Fig. 76. Temperatures in Average Oxide-fuel Subassembly following the Driving of a Central Subassembly at High Speed into a Just-critical Core; Doppler Constant = -0.0005; Half of Metal-fuel Feedback; Reduced Coolant Flow. ANL Neg. No. ID-103-M5757.

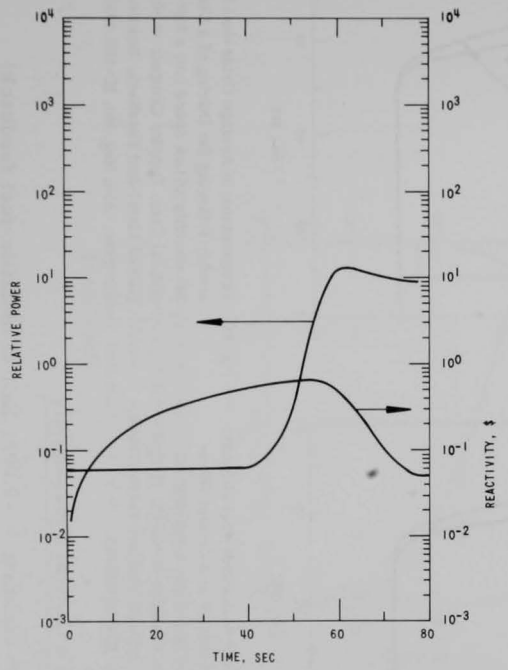

Fig. 77. Power and Reactivity Curves following the Driving of a Central Subassembly at Low Speed into a Just-Critical Core; Doppler Constant = -0.002; Half of Metal-fuel Feedback; Reduced Coolant Flow. ANL Neg. No. ID-103-M5758.

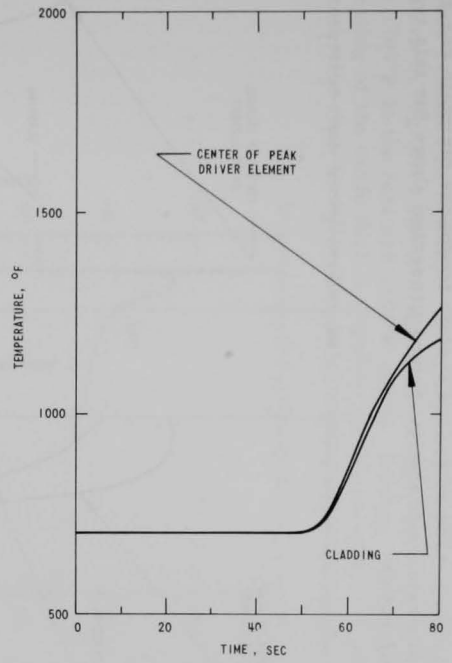

Fig. 78. Temperatures in Peak Driver-fuel Element following the Driving of a Central Subassembly at Low Speed into a Just-critical Core; Doppler Constant = -0.002; Half of Metal-fuel Feedback; Reduced Coolant Flow. ANL Neg. No. ID-103-M5759.

the cladding. The temperatures in the peak oxide-fuel element are slightly higher, reaching 1600°F in the fuel and 1450°F on the cladding (see Fig. 79). The average oxide-fuel temperatures, as shown in Fig. 80, lie between the peak metal and oxide temperatures, with values of 1490°F in the fuel and 1390°F on the cladding. The increased system feedbacks maintain reactivity and material temperatures to the low values presented above for this type of hypothetical malfunction.

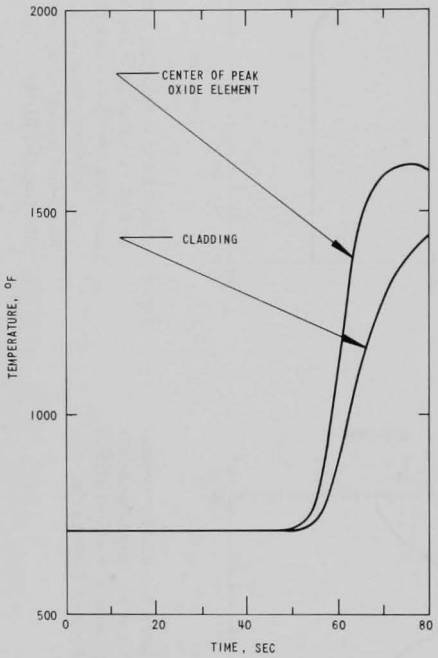

Fig. 79. Temperatures in Peak Oxide-fuel Element following the Driving of a Central Subassembly at Low Speed into a Just-critical Core; Doppler Constant = -0.002; Half of Metal-fuel Feedback; Reduced Coolant Flow. ANL Neg. No. ID-103-M5760.

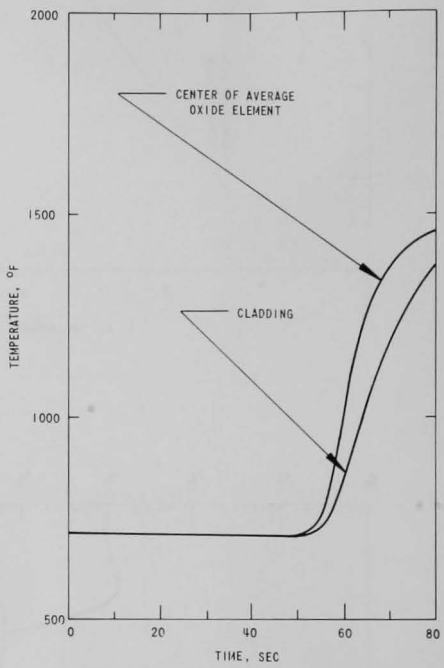

Fig. 80. Temperatures in Average Oxide-fuel Subassembly following the Driving of a Central Subassembly at Low Speed into a Just-critical Core; Doppler Constant = -0.002; Half of Metal-fuel Feedback; Reduced Coolant Flow. ANL Neg. No. ID-103-M5761.

3. Dropping of a Central Subassembly

(Doppler constant = -0.002; half of metallic-fuel feedback)

This hypothetical malfunction is prevented by numerous levels of redundant controls, but since this malfunction is mentioned in the EBR-II Hazard Summary Report,[1,2] an analysis with Doppler feedback is

presented. The power and reactivity curves following this insertion, as shown in Fig. 81, indicate that the reactor would be prompt critical for a short time. Peak driver-fuel-element temperatures (plotted in Fig. 82) reach 1800°F in the fuel and 1700°F on the cladding. Peak oxide temperatures remain low at 2200°F in the fuel and 1200°F on the cladding, as shown in Fig. 83. The average oxide temperatures (Fig. 84) are even lower at 1700°F in the fuel and 1100°F on the cladding. Owing to the rapid rate of heating of the oxide fuel, a Doppler coefficient affords a greater degree of protection than metallic-fuel axial expansion in this case.

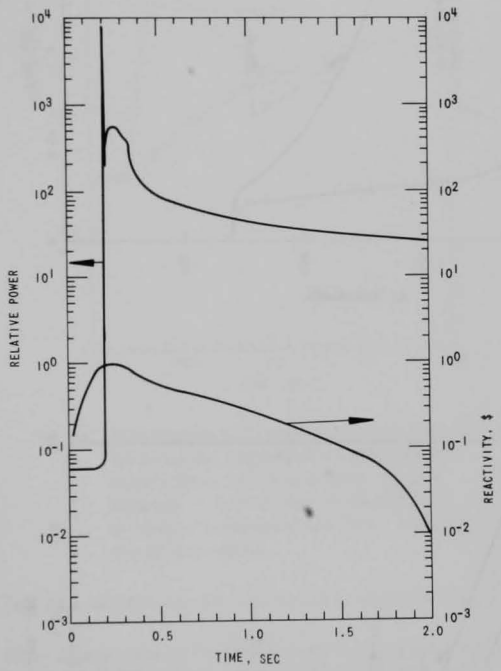

Fig. 81. Power and Reactivity Curves following the Dropping of a Central Subassembly into a Just-critical Core; Doppler Constant = -0.002; Half of Metal-fuel Feedback; Reduced Coolant Flow. ANL Neg. No. ID-103-M5762.

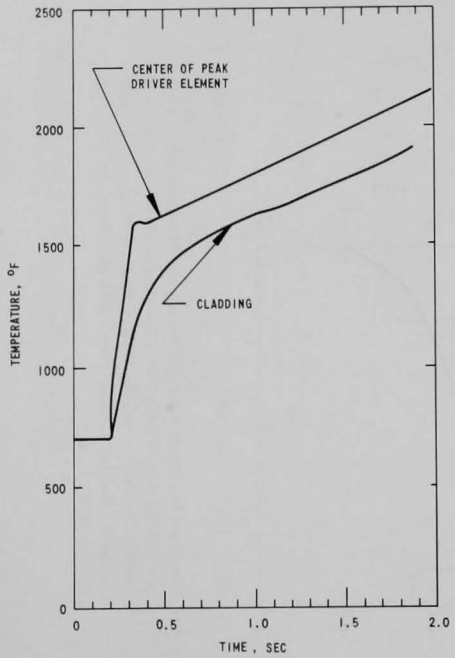

Fig. 82. Temperatures in Peak Driver-fuel Element following the Dropping of a Central Sub-assembly into a Just-critical Core; Doppler Constant = -0.002; Half of Metal-fuel Feedback; Reduced Coolant Flow. ANL Neg. No. ID-103-M5763.

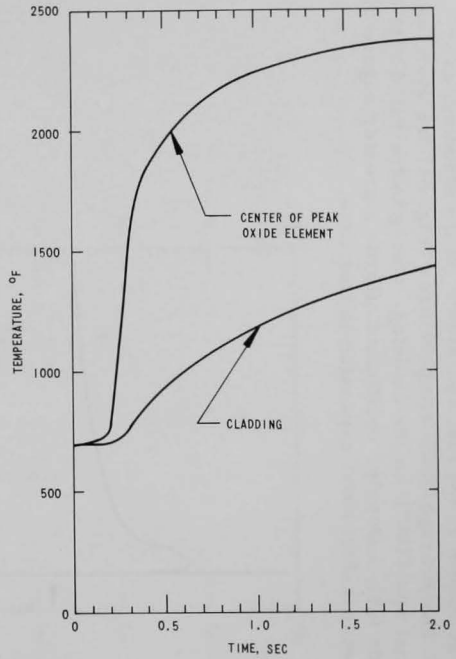

Fig. 83. Temperatures in Peak Oxide-fuel Element following the Dropping of a Central Sub-assembly into a Just-critical Core; Doppler Constant = -0.002; Half of Metal-fuel Feedback; Reduced Coolant Flow. ANL Neg. No. ID-103-M5764.

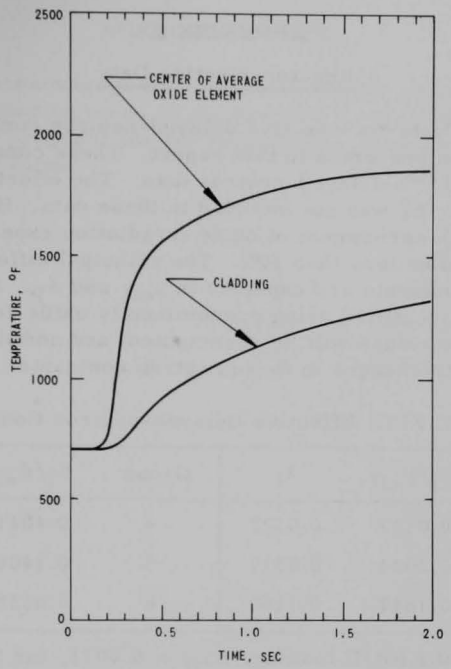

Fig. 84. Temperatures in Average Oxide-fuel Element following the Dropping of a Central Subassembly into a Just-critical Core; Doppler Constant = -0.002; Half of Metal-fuel Feedback; Reduced Coolant Flow. ANL Neg. No. ID-103-M5765.

Results for the above three cases are summarized in Table XIII.

TABLE XIII. Comparison of Various Reactivity-feedback Effects on Peak Fuel-element Temperatures following Fuel-handling Malfunctions

Case No.	Feedback from Driver-fuel Element		Feedback from Oxide-fuel Element		Temperatures in Peak Driver-fuel Element		Temperatures in Peak Oxide-fuel Element	
	Fuel, $/°F	Coolant, $/°F	Fuel, $T\frac{\partial k}{\partial T}$	Coolant, $/°F	Fuel, °F	Cladding, °F	Fuel, °F	Cladding, °F
1	-0.000189	-0.006800	-0.0005	-0.00621	1800[a]	1750[a]	2250[a]	1490[a]
2	-0.000189	-0.00680	-0.002	-0.00621	1250[b]	1200[b]	1600[b]	1450[b]
3	-0.000189	-0.00680	-0.002	-0.00621	1800[c]	1700[c]	2200[c]	1200[c]

[a]10 sec after start of insertion.
[b]80 sec after start of insertion.
[c]1 sec after start of insertion.

APPENDIX B

Reactor-kinetics Data

Table XIV lists the effective delayed-neutron constants used in the dynamic simulation presented in this report. These constants are obtained using only ^{235}U and ^{238}U delayed-neutron data. The effect of ^{239}Pu or ^{240}Pu in oxide fuel on the β_i was not included in these data. However, owing to the anticipated high enrichment of oxide irradiation experiments, the induced error should be less than 10%. The principal differences from present nuclear constants are expected in β_{eff} and ℓ_p. As more definitive core loadings are identified using predominantly oxide-fuel irradiation experiments, these values will be recomputed, and additional studies will be made to evaluate changes in these neutron constants.

TABLE XIV. Effective Delayed-neutron Constants

Group	β_i/β_{eff}	λ_i	Group	β_i/β_{eff}	λ_i
1	0.0347	0.0127	4	0.4041	0.3110
2	0.2034	0.0317	5	0.1406	1.4000
3	0.1847	0.1150	6	0.0325	3.8700

For present EBR-II loading, β_{eff} = 0.0071; for 50% EBR-II driver fuel and 50% mixed-oxide fuel, β_{eff} = 0.0066; for 100% mixed-oxide fuel, β_{eff} = 0.0056.
$\ell_p = 1.10 \times 10^{-7}$ sec.

ACKNOWLEDGMENT

I wish to acknowledge the analytical support provided by I. A. Engen in preparing many of the dynamic system analyses for the AIROS-IIA digital program and for reproducing many of the analytical results in graphic form.

REFERENCES

1. L. J. Koch, H. O. Monson, D. Okrent, M. Levenson, W. R. Simmons, J. R. Humphreys, J. Haugsnes, V. C. Jankus, and W. B. Loewenstein, *Hazard Summary Report, Experimental Breeder Reactor II (EBR-II)*, ANL-5719 (May 1957).

2. L. J. Koch, W. B. Loewenstein, and H. O. Monson, *Addendum to Hazard Summary Report, Experimental Breeder Reactor II (EBR-II)*, ANL-5719 (Addendum) (June 1962).

3. J. C. Case, *Core-loading Diagrams for EBR-II, Runs 4 through 38 (April 1965 through Mid-December 1969)*, ANL/EBR-007 (Dec 1969).

4. A. V. Campise, *Dynamic Simulation and Analysis of EBR-II Rod-drop Experiments*, ANL-7664 (Mar 1970).

5. A. V. Campise, *A Study of the Response of the EBR-II Plant Protective System to Hypothetical Malfunctions in the Reactor System*, ANL-7665 (June 1970).

B